Université Libre de Bruxelles

BRUFACE
BRUSSELS FACULTY OF ENGINEERING

Master Thesis

DESIGN OF A HYDROGEN BLENDED WING BODY AIRCRAFT FOR LONG RANGE TRANSPORTATION

Student:

Diego Jordá Espí (diego.jorda.espi@ulb.be)

Academic year 2022-2023

Master thesis submitted under the supervision of Prof Patrick Hendrick, in order to be awarded the Master's Degree in Aeronautical Engineering.

ULB UNIVERSITÉ LIBRE DE BRUXELLES

ULB UNIVERSITÉ LIBRE DE BRUXELLES

Exemplaire à apposer sur le mémoire ou travail de fin d'études,
au verso de la première page de couverture.

Fait en deux exemplaires, **Bruxelles, le 16/08/2023**

Réservé au secrétariat : **OUI** **NON**

CONSULTATION DU MEMOIRE/TRAVAIL DE FIN D'ETUDES

Je soussigné

NOM :
Jordá Espí

PRENOM :
Diego

TITRE du travail :
DESIGN OF A HYDROGEN BLENDED WING BODY AIRCRAFT FOR LONG RANGE TRANSPORTATION

REFUSE

la consultation du présent mémoire/travail de fin d'études par les utilisateurs des bibliothèques de l'Université libre de Bruxelles.

Si la consultation est autorisée, le soussigné concède par la présente à l'Université libre de Bruxelles, pour toute la durée légale de protection de l'œuvre, une licence gratuite et non exclusive de reproduction et de communication au public de son œuvre précisée ci-dessus, sur supports graphiques ou électroniques, afin d'en permettre la consultation par les utilisateurs des bibliothèques de l'ULB et d'autres institutions dans les limites du prêt inter-bibliothèques.

Abstract

Master's thesis: Design of a hydrogen blended wing body aircraft for long range transportation.

Author: Diego Jordá Espí.

Academic year 2022-2023.

In December 2019, the European Commission put forth its Green Deal with the objective for decarbonization: net carbon neutrality across all sectors and EU member states by 2050. This means that the aviation sector must decarbonize, and do it so quickly. Most efforts have focused on the use of liquid hydrogen as a fuel, due to its high specific energy and its zero CO2 emissions.

The aim of this study is to analyze the advantages of the BWB design over the conventional one with the introduction of this fuel. The impact of the LH2 in current aircraft is analyzed through structural, energy and aerodynamic efficiencies. In addition, a Blended Wing Body aircraft will be designed for long range transportation using hydrogen as fuel, and its performance will be compared to the existing A350-1000.

Results show that the new configuration has an increase of 27% in aerodynamic efficiency due to its reduced wetted area. This suggests that BWB aircraft are optimal to counteract the drawbacks of the use of hydrogen as fuel. However, improvements in the hydrogen storage system must take so that the introduction of this fuel is possible in the aerospace sector and to improve the performance of aircraft.

Keywords: LH2, BWB, Conceptual design, zero emissions, long range.

Acknowledgement

Six years ago I made the decision to establish a link with the aeronautical world. It was my calling, and what I felt I had to do at the time. After all this journey, I feel that it is necessary to dedicate this work to my family, for putting up with me and encouraging me throughout my life, without ever letting me give up.

Also, I would like to thank my friends from the university, for making these six years the best years possible.

And I can't forget the friends I've made this year in Brussels. It has been a year full of new experiences, challenges, life lessons... Without them everything would have been very different, and I am very grateful for everything I have learned with them.

Thank you all!

Contents

Abstract III

Acknowledgements V

List of Figures VIII

List of Tables X

1 Introduction 1

1 Structural efficiency . . . 3

1.1 Short range aircraft . . . 4

1.2 Long-range aircraft . . . 6

2 Energy efficiency . . . 9

3 Aerodynamic efficiency . . . 11

2 Reverse engineering 12

1 Similar aircraft . . . 12

1.1 A350-1000 . . . 12

1.2 X-48B . . . 14

1.3 Airbus MAVERIC . . . 15

2 Mission profile . . . 16

3 Reverse engineering . . . 16

3.1 Flight conditions . . . 17

3.2 Basic geometry . . . 17

3.3 Aerodynamics . . . 17

3.4 Weights . . . 24

3.5 Estimation of propulsion system . . . 25

3.6 Estimation of performance . . . 26

3 The new BWB aircraft **30**
1 Initial sizing . . . 30
1.1 Weight estimation . . . 30
1.2 Geometry and aerodynamics . . . 33
2 Aerodynamics . . . 35
2.1 TORNADO VLM . . . 35
2.2 Sensitivity analysis . . . 36
3 Refined weights . . . 38
3.1 Center of gravity . . . 40
4 Engine selection . . . 41
5 Vertical tails . . . 42
5.1 Horizontal tails . . . 45
6 Take-off and landing distances . . . 46
6.1 Take-off distance . . . 46
6.2 Landing distance . . . 48
7 Restrictions . . . 50
7.1 Cruise . . . 50
7.2 Take-off . . . 50
7.3 Climb . . . 51
7.4 Landing . . . 51
7.5 Results . . . 52
8 Internal dimensioning . . . 52
8.1 Passengers cabin . . . 53
8.2 Fuel tanks . . . 55
9 Estimation of performance . . . 56

4 Conclusion **58**

Bibliography **60**

List of Figures

1.1 Structural efficiency evolution with $W_{initial}/W_{final}$. 4
1.2 ZFW vs Structural Efficiency diagram. 6
1.3 Structural efficiency vs GI. 6
1.4 Structural efficiency vs ZFW diagram. 8
1.5 Structural efficiency evolution with GI. 8
1.6 Location of new LH2 tanks [8]. 11

2.1 Picture of an A350-1000 [13]. 13
2.2 X-48B [17]. 14
2.3 Airbus MAVERIC [19]. 15
2.4 Mission profile of the A350-1000. 16
2.5 Fineness ratio of the fuselage. 22
2.6 Contribution to the C_{D_0} per component. 24
2.7 Reverse engineering parameter evolutions (I). 27
2.8 Reverse engineering parameter evolutions (II). 28
2.9 Reverse engineering parameter evolutions (III). 28

3.1 Comparision of three blending parts. 34
3.2 The different fidelity levels for aerodynamics solvers. 35
3.3 Lattice in Tornado VLM. 36
3.4 Diagram for the calculation of CoG. 40
3.5 Force and moment diagram. 42
3.6 Construction sketch of the vertical tail. 44
3.7 Control surfaces for pitch and roll. 45
3.8 Performance (restrictions). 52
3.9 Distribution of the floors. 53
3.10 Design parameters of the seat. 53

3.11 Distribution of half toilet. 54
3.12 Internal distribution of the cabin 54
3.13 Location of the different fuel tanks. 55
3.14 New design parameter evolutions (I). 56
3.15 New design parameter evolutions (II). 56
3.16 New design parameter evolutions (III) 57

4.1 Views of the final design. 59

List of Tables

1.1 Thermodynamic properties of different fuels. . . . 3
1.2 A320's weights [5]. . . . 5
1.3 Results for a short-range aircraft. . . . 5
1.4 A350-1000 weight specifications [6]. . . . 7
1.5 Study results for long-range aircraft. . . . 7
1.6 Design parameters of turbofans analyzed [7] 10
1.7 Energy efficiency results. . . . 10

2.1 Basic geometrical parameters of Airbus Maveric and X-48B. . . . 16
2.2 A350's geometrical parameters. . . . 18
2.3 NASA SC(2)-0714 2D data. . . . 18
2.4 NACA 0012 2D data. . . . 19
2.5 A350-1000 lift-related coefficients (main wing). . . . 20
2.6 A350 weight distribution. . . . 24
2.7 RR Trent XWB's reference values. . . . 26

3.1 Geometry parameters of BWB. . . . 33
3.2 NACA 4418 2D data. . . . 34
3.3 Data of the three prototypes. . . . 34
3.4 Results of the sensitivity analysis. . . . 37
3.5 Geometry of the final aircraft. . . . 37
3.6 Design parameters of the seat. . . . 53

CHAPTER 1

Introduction

In December 2019, the European Commission put forth its Green Deal with the objective for decarbonization: net carbon neutrality across all sectors and EU member states by 2050. For aviation, this target is even more ambitious than those from the Air Transport Action Group (ATAG), which call for carbon-neutral growth from 2020 onwards and a 50 percent reduction of emissions by 2050 relative to 2005 levels. Both targets put the aviation sector under increasing pressure to decarbonize – and do so quickly. [1]

Per passenger, aviation sector has become more efficient in terms of greenhouse emissions. Fuel efficiency per revenue passenger kilometer has increased about 50% due to high seat density, operational improvements and technology improvements. However, rising demand for air transport has led to a significant increase in CO2 emissions from aviation. Growing populations and economies will heavily increase the demand in such a way that, assuming industry growth of 3 to 4 percent per year, and efficiency improvement of 2% per year, emissions would be more than double by 2050. Greenhouse emissions not only include CO2, but also nitrogen oxides (NOX), soot, and water vapor. These ones create contrails and cirrus clouds, so the aim is not to only decrease CO2 emissions, but all emissions that contribute to global warming. [1]

To reduce the climate impact of aviation and reach the objectives of European Commission and ATAG, industry will have to change the type of fuel. To date, most efforts have focused on the development of Sustainable Aviation Fuels (SAFs). However, its development has been

slow due to limited supply and high cost. In fact, SAF fuels only represent 0.05% of global jet fuel use in 2021. Nevertheless, their advantages are clear: they are drop-in fuels that can be blended up to 50% in existing aircraft and have similar energy per unit volume as kerosene fuel. Their problem is that they still emit CO2 when burnt. [2]

SAF can be classified in two groups: biofuels and synfuels. Biofuels are produced from organic material such as trees, plants, and agricultural and urban waste. Depending on which type of biomass is used, they could lower CO2 emissions by 20-98% compared to conventional jet fuel. In contrast to biofuels, the main source of synfuels is electricity. Electricity is used to first produce hydrogen and to capture carbon, combining the two into a kerosene-like fuel.

Aviation industry is also exploring alternative propulsion technologies, like electric propulsion systems that can be distributed or integrated in fuselage and hydrogen. On one hand, electric propulsion's main disadvantage are limitations in battery energy per unit of mass (specific energy) that has a penalty on the aircraft's range, and therefore, the potential market share of electric aircraft. On the other hand, hydrogen is a promising alternate energy source due to its high energy content per unit of mass (specific energy) and because a clear pathway to zero-emission production exists, using entirely renewable electricity ("green hydrogen") [2].

As for hydrogen, depending on the process used to extract it, it can be considered as a renewable or non-renewable source. Hereby, the hydrogen colour code was created, where there are different types, from green hydrogen (the most renewable one) to black hydrogen (with the most polluting processes). The two best-known colours are blue hydrogen and the green one. The process for obtaining blue hydrogen involves hydrocarbons, and through a chemical process it is obtained hydrogen on the one hand, and carbon dioxide on the other. Green hydrogen is obtained by separating hydrogen from oxygen through the electrolysis of water. This electrolysis can be carried out with energy from renewable sources, which makes the process sustainable and clean. It is a pollutant-free process. [3]

Table 1.1 lists the thermodynamic properties of Jet A, e-Kerosene (SAF), compressed gaseous H2 and liquid H2. A significant challenge for hydrogen-powered aircraft designs is fuel storage. Jet A can be stored in integral tanks within the wing structure, and in fuselage tanks. Hydrogen stores 2.8 times the energy per unit of mass of Jet A. However, its volumetric energy density is much lower. The main issue is that producing the energy of a unit of volume of Jet A requires 7 times that volume of compressed GH2 and 4 times that volume of LH2. This makes LH2 a better choice from the perspective of improving the payload capacity and range of potential H2-powered aircraft. [2]

To understand how the change in fuel can affect the range and aircraft performance, Breguet's equation must be considered.

Properties	Units	Jet A	e-Kerosene	GH2	LH2
LHV	MJ/kg	43	43 $(1x)$	120 $(2.8x)$	120 $(2.8x)$
ρ	kg/m^3	808	808 $(1x)$	42 $(0.05x)$	71 $(0.09x)$
$Energy$ $density$	GJ/m^3	34.7	34.7 $(1x)$	5 $(0.14x)$	8.5 $(0.25x)$

Table 1.1: Thermodynamic properties of different fuels.

Breguet's equation:

$$Range = \frac{V \cdot \frac{L}{D}}{g \cdot TSFC} \cdot ln\left(\frac{W_{initial}}{W_{final}}\right) \tag{1.1}$$

There are three terms that must be studied:

- Energy efficiency: $\frac{1}{TSFC}$
- Structural efficiency: $ln\left(\frac{W_{initial}}{W_{final}}\right)$
- Aerodynamic efficiency: $\frac{L}{D}$

1 Structural efficiency

Structural efficiency is linked to the mass of weight that is consumed during the flight. It appears in the Breguet's equation as the logarithm of the initial weight divided by the final weight: $ln\left(\frac{W_{initial}}{W_{final}}\right)$.

Figure 1.1 shows how this efficiency evolves with the ratio $\frac{W_{initial}}{W_{final}}$. This means the more weight is consumed during the flight, the better structural efficiency, and thus, longer range. So when designing an aircraft, the difference between Take-off Weight and Zero Fuel Weight must be as high as possible. LH2 has the drawback of a low density (kg/m^3), so to carry the same amount of mass than Jet A, a much higher volume of storage is needed. This implies big LH2 storage tanks, which are heavier than Jet A ones and increase the ZFW.

To see the effect of adding these tanks to the aircraft, a study has been carried out comparing the structural efficiency of a short-range aircraft and a long-range aircraft with kerosene and with LH2 . Note that aircraft designs aren't changed. The short-range aircraft is an A320 and the long-range aircraft is an A350-1000.

They are studied for five cases, one for kerosene and the other four for LH2:

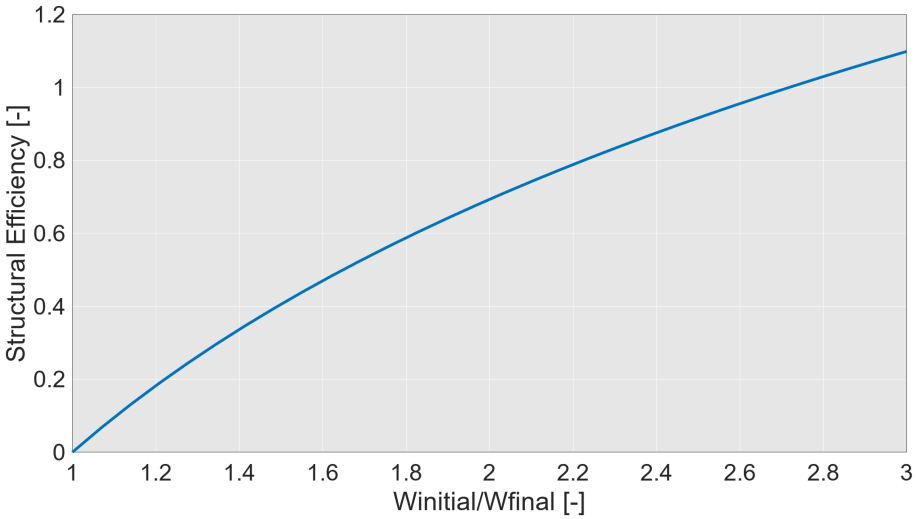

Figure 1.1: Structural efficiency evolution with $W_{initial}/W_{final}$.

- Case 0: aircraft use Jet A fuel and tanks are filled until reaching $V_{fuel,max}$ or $MTOW$.
- Case 1: aircraft carry the same amount of energy as in Case 0 using LH2.
- Case 2: LH2 is used and contained in the same amount of volume as in Case 0.
- Case 3: LH2 weight equals Jet A fuel's weight in Case 0.
- Case 4: aircraft take-off with TOW = MTOW using LH2.

To consider the effect of the tanks, heat exchangers and fuel delivery components a new variable has been added. This one is the 'Gravimetric Index' (GI). This variable is the ratio between the fuel mass and the total dry fuel system mass. Jet A can achieve a very high GI (about 1.0) as integral fuel tanks are built into the structure of the wing. For LH2, this value will be much lower. While structural and thermal analysis suggests that a fuel tank of GI between 0.5 and 0.8 can be achieved for LH2 [4], this analysis will use a GI of 0.35 assuming an evolutionary (not revolutionary) evolution of designs [2].

$$GI = \frac{W_{fuel}}{W_{fuel} + W_{dry\ fuel\ system}} \tag{1.2}$$

1.1 Short range aircraft

The A320 is a twin-engine jet manufactured by Airbus Industries used for short-range missions. Table 1.2 shows the weight specifications of this aircraft. For the payload weight, it's assumed that each passenger has an associated weight of $100\ kg$ (due to its own weight and luggage).

The study is performed and results are obtained in Table 1.3. It is seen that Case 1 and Case 3 are not feasible as they exceed the MTOW. For the kerosene case, the Structural

Operational Empty Weight	$42600\,kg$
MTOW	$78000\,kg$
Payload	$15000\,kg$
Maximum Fuel Volume	$27.2\,m^3$

Table 1.2: A320's weights [5].

Efficiency is 0.30319, the highest possible as the Gravimetric Index for this type of fuel is 1. The LH2 cases have a lower efficiency, being the Case 4 the optimal one. In this case, its efficiency is 0.096, which means a 31.663% of the kerosene one. In other words, the efficiency has a reduction of 0.2072. This will lead to a reduction of the aircraft's range. In addition, it is seen that for Case 4 the volume of fuel stored is about four time the one with kerosene. This can lead to a discussion about whether it is possible or not, as fuselage is not changed, LH2 tanks will occupy space in the fuselage destined to payload (LH2 tanks cannot be stored in wings), reducing the revenues of the airline and increasing costs. So the most realistic case is the 2 one, but its Structural Efficiency is too low compared to the Jet A fuel: just a 0.028996.

A320	Case 0	Case 1	Case 2	Case 3	Case 4
$W_{tanks}\,(kg)$	-	13576	3329.1	37886	13260
$V_{fuel}\,(m^3)$	25.248	102.96	25.24	287.32	100.56
$W_{fuel}\,(kg)$	20400	7310	1792.6	20400	7140
$W_{to}\,(kg)$	78000	78486	62722	115890	78000
$W_{final}\,(kg)$	57600	71176	60929	95486	70860
$Energy\,carried\,(MJ)$	877200	877200	215110	2448000	856800
Structural Efficiency	**0.30319**	**0.0978 (32,26%)**	**0.028996 (9.5636%)**	**0.1936 (63.85%)**	**0.096 (31,663%)**

Table 1.3: Results for a short-range aircraft.

Figure 1.4 shows the diagram of Structural Efficiency vs Zero Fuel Weight, which is analogous to the payload-range diagram. In that figure the blue line represents the kerosene case, and the red one the LH2 case. Both cases are studied for the same TOW (TOW = MTOW) and full consumption of the fuel. It is seen that for the kerosene case you can achieve a higher increase in Structural Efficiency than for LH2 case when reducing the payload.

Note that this diagram consists of three zones. In the first one, the full payload is loaded, and the fuel tanks are filled until reaching MTOW. In the second one, the payload weight decreases and the fuel weight increases until reaching the maximum volume. The last phase is characterized by the reduction of payload weight, while the fuel is the maximum possible.

Figure 1.5 shows the evolution of the Structural efficiency with the Gravimetric Index,

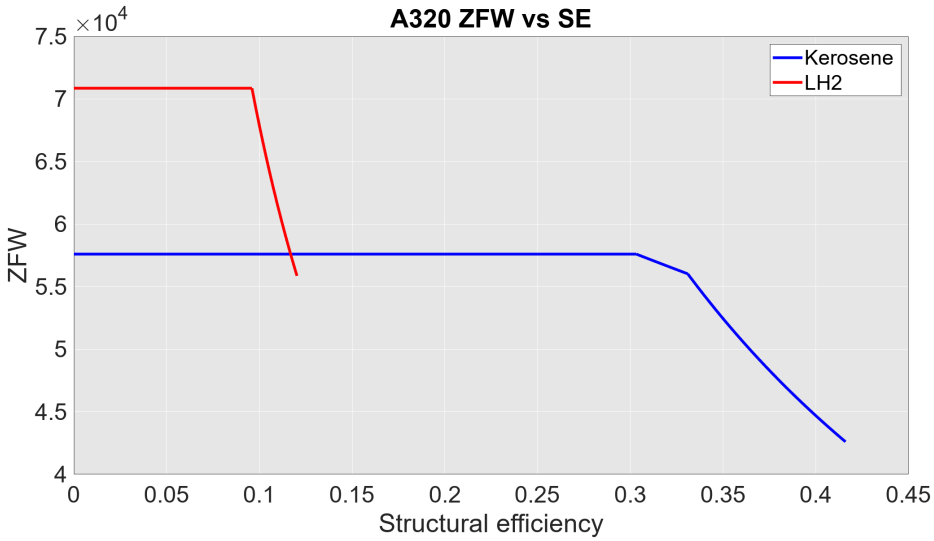

Figure 1.2: ZFW vs Structural Efficiency diagram.

assuming that LH2 aircraft takes-off with the same weight as in Case 0. It is seen that it has a linear shape. In addition, the Gravimetric Index must be 1 so that the efficiency is equal to the kerosene case.

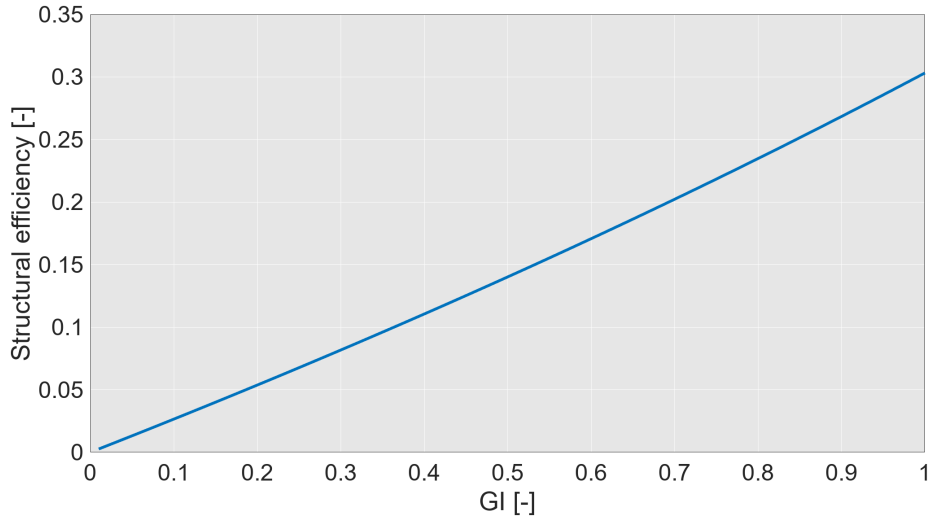

Figure 1.3: Structural efficiency vs GI.

1.2 Long-range aircraft

The A350-1000 is a long-range, wide-body twin-engine jet airliner developed and produced by Airbus. It has the ability of carrying 369 passengers and has a maximum range of $16100\ km$.

Table 1.4 shows the weight specifications of this aircraft. Payload weight has been calculated as in short-range case (assuming $100\ kg$ per passenger).

Operational Empty Weight	$155000\ kg$
MTOW	$319000\ kg$
Payload	$36900\ kg$
Maximum Fuel Volume	$158.79\ m^3$

Table 1.4: A350-1000 weight specifications [6].

Study is performed and Table 1.5 shows its results.

A350	Case 0	Case 1	Case 2	Case 3	Case 4
$W_{tanks}\ (kg)$	–	84582	20741	236040	82615
$V_{fuel}\ (m^3)$	157.3	641.47	157.3	1790.1	626.55
$W_{fuel}\ (kg)$	127100	45544	11168	127100	44485
$W_{to}\ (kg)$	319000	322030	223810	555040	319000
$W_{final}\ (kg)$	191900	276480	212640	427940	274515
$Energy\ carried\ (MJ)$	5465300	5465300	1340200	15252000	5338200
Structural Efficiency	**0.50822**	**0.15249** (30.183%)	**0.05119** (10.07%)	**0.26006** (51.171%)	**0.15019** (29.552%)

Table 1.5: Study results for long-range aircraft.

Note that Case 1 and 3 are not feasible as they exceed the MTOW. Case 4 is the optimal one with a Structural Efficiency of 0.15019 (29.552% of the kerosene one), but it has the same problem as in short-range: fuel volume is four times bigger. Case 2 is the most realistic one, but its Structural Efficiency is very poor: just 0.05119, which corresponds to a 10.07% of the Case 0 one. In all cases, the structural efficiency reduces more than in the short-range case, but the ratio it reduces is more or less similar (except for the Case 3). Figure 1.4 shows the diagram of Structural Efficiency vs Zero Fuel Weight, where the blue line represents the kerosene case, and the red one the LH2 case. Both cases are studied for the same TOW (TOW = MTOW). It is seen that for the kerosene case you can achieve a higher increase in Structural Efficiency than for LH2 case when reducing the payload.

Figure 1.5 shows the evolution of the Structural efficiency with the Gravimetric Index, assuming that LH2 aircraft takes-off with the same weight as in Case 0. It is seen that it has a linear shape, as in the short-range case. In addition, the Gravimetric Index must be 1 so that the efficiency is equal to the kerosene case.

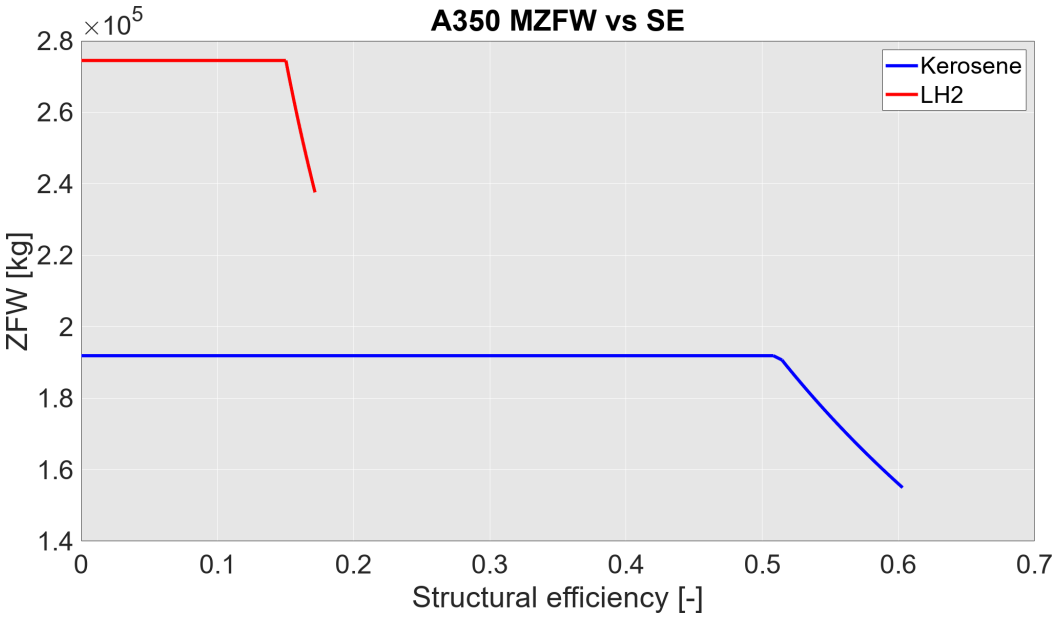

Figure 1.4: Structural efficiency vs ZFW diagram.

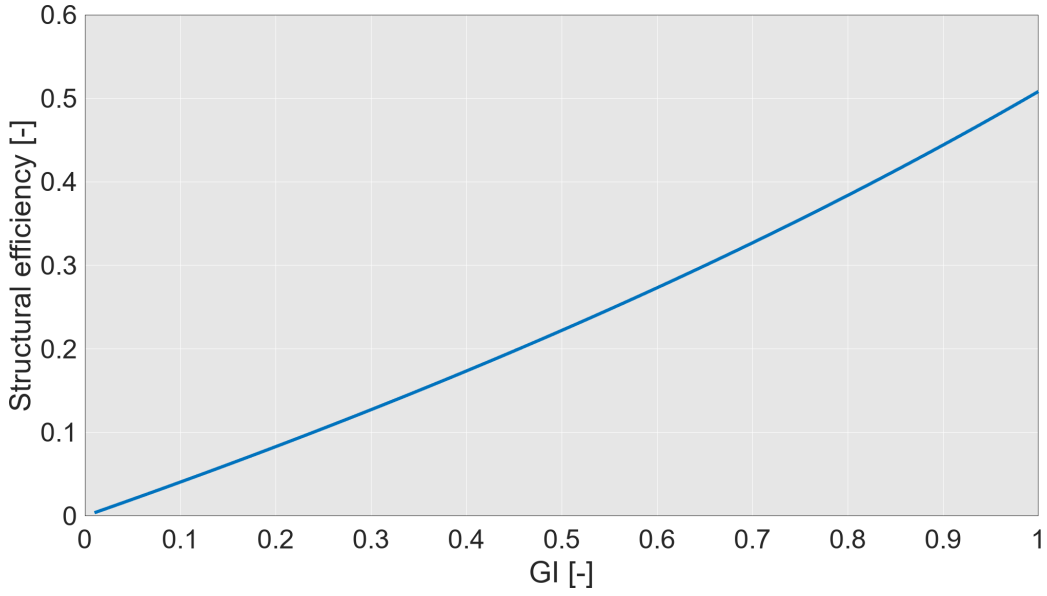

Figure 1.5: Structural efficiency evolution with GI.

2 Energy efficiency

The energy efficiency is linked to the fuel mass consumption. As LH2 has a higher LHV, less fuel mass is consumed per second. However, it also depends on other parameters like the c_p of the gas mixture (LH2 and air) and the efficiency of the combustion chamber (η_{cc}).

To study with accuracy this parameter, the software called *GasTurb* has been used. This program allows to design and simulate gas turbines, which are are engines that transform thermal energy into mechanical energy, and they are used in the energy sector and aerospace engineering. Engineers can model and simulate a number of gas turbine functions, including power generation, exhaust gas expansion, fuel combustion, and air compression, using *GasTurb*. The program offers resources for both analyzing and enhancing existing designs as well as for creating brand-new gas turbine designs. The main features of this program are:

- Thermodynamic analysis: Allows detailed calculations of the thermodynamic processes that occur within a gas turbine, such as efficiency, compression ratio, exhaust gas temperature, etc.
- Design and optimization: Enables the design and optimization of gas turbines by selecting design parameters such as rotor and stator geometry, blade profiles, entry and exit angles, etc.
- Combined Cycle Analysis: Allows you to simulate and analyze the operation of gas turbines in combined cycle systems, where both gas turbines and steam turbines are used to increase overall efficiency.
- Performance Analysis: Provides tools to evaluate and compare the performance of different gas turbine configurations, taking into account factors such as efficiency, fuel consumption, emissions, etc.

For the short-range study, the turbofan analyzed will be the CFM56-5B4, as it is the one used by the A320-214. As for the long-range study, the Rolls Royce Trent XWB will be used, as it is used in the A350-1000. Their specifications are given in Table 1.6. It can be seen that the CFM56 is older than Trent XWB, as it has a relatively low bypass ratio for a turbofan used in commercial aviation. Concretely, the CFM56-5B4 is from 1995 and the XWB is from 2010. Both engines will be analyzed in Static Sea Level (SSL) conditions, as it was really difficult to obtain those parameters in cruise conditions.

Both engines were simulated using *GasTurb*, and the results were obtained in Table 1.7.

It is seen that using LH2, the Thrust at SSL increases a bit, but the most important change

Design parameters	CFM56-5B4	Rolls-Royce Trent XWB
Type of turbofan	Two spools TF	Three spools TF
Intake pressure ratio	0.99	0.99
Inner fan pressure Ratio	2.5	1.3
Outer Fan pressure Ratio	1.8	1.3
IP Compressor pressure Ratio	-	5.5
HP Compressor pressure Ratio	6.466	5.4
OPR	29.1	50
Bypass duct pressure Ratio	0.98	0.98
Bypass Ratio	5.7	9.6
Burner Exit Temperature (K)	1450	1800
Isentr. Inner LPC Efficiency	0.9	0.88
Isentr. Outer LPC Efficiency	0.91	0.88
Isentr. IPC Efficiency	-	0.85
Isentr. HPC Efficiency	0.88	0.86
Isentr. HPT Efficiency	0.89	0.9
Isentr. IPT Efficiency	-	0.92
Isentr. LPT Efficiency	0.89	0.91

Table 1.6: Design parameters of turbofans analyzed [7] .

Results	Units	CFM56-5B4		Rolls-Royce Trent XWB	
Fuel		Jet A	LH2	Jet A	LH2
Thrust	kN	129.86	$135.19\ (1.04\,x)$	376	$384\ (1.02\,x)$
mf	kg/s	1.3463	$0.5041\ (0.374\,x)$	3.784	$1.4431\ (0.381\,x)$
TSFC	$kg/(daN \cdot s)$	0.3732	$0.1342\ (0.359\,x)$	0.3623	$0.1353\ (0.373\,x)$

Table 1.7: Energy efficiency results.

is the reduction in the fuel burnt. This will lead to a reduction in the TSFC, which means a big improvement of the energy efficiency. Concretely, the thrust has increased a 4% in the CFM56 and a 2% in the Trent XWB changing the fuel to hydrogen. The fuel burnt was reduced a 62.55% and 61.85% for the CFM56 and XWB, respectively. Finally, the TSFC for the CFM56 using LH2 is 0.359 times the one using kerosene fuel type, and 0.373 also for the Trent XWB. In future calculations, it will assumed that the TSFC for engines that use hydrogen is 0.36 the one using Jet A.

3 Aerodynamic efficiency

The last term to be analyzed from the Breguet equation is the aerodynamic efficiency. This is the Lift produced by the aircraft divided by the Drag. Most studies are focused on adding hydrogen on current aircraft (Tube and Wing configuration), and as hydrogen can't be stored in wings, they would require extra tanks with extra space and fuselage, as seen in Figure 1.6.

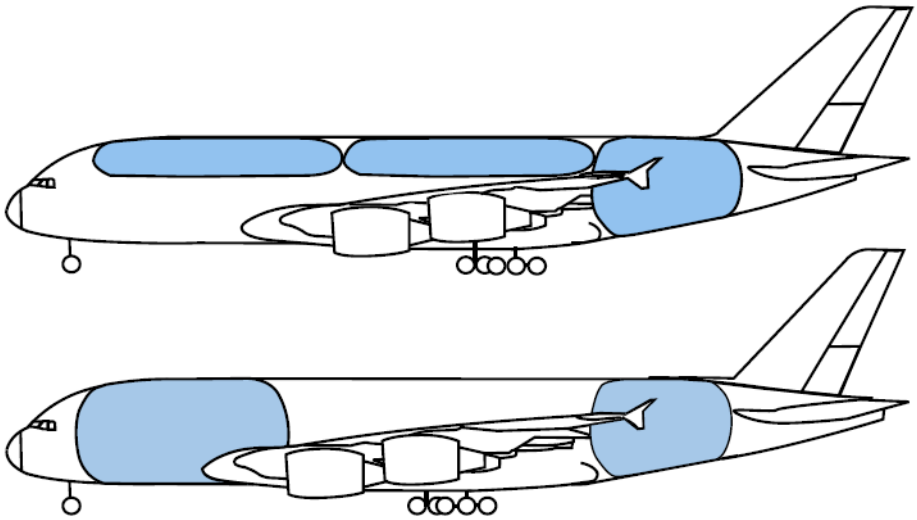

Figure 1.6: Location of new LH2 tanks [8].

Drag depends on the wetted area of the flying body. By increasing the fuselage volume, the wetted area will increase, and also the Drag. As a consequence, the aerodynamic efficiency will decrease, which has a negative impact in the Breguet equation and the flight mechanics of the aircraft.

However, there's an aircraft configuration that allows an increase in the inner volume with a lower wetted surface area when compared to the 'Tube and Wing' configuration. This one is called 'Blended Wing Body' aircraft. According to Torenbeek [9], using this configuration fuel efficiency improvements between 30% and 40% can be expected. This is also reasserted by Chen et al[10], as the fuel efficiency is 31.5% better than TAW. Finally, using BWB less polutants are emited due to reduced fuel burn and propulsive efficieny, the range and payload capacity are increased due to 27% of fuel burn per seat, and the aerodynamic efficiency is increased by $15 - 20\%$ because it implies 33% lower wetted surface area [11]. So the aim of this Master thesis is the design of a Blended Wing Body aircraft for the long-range commercial transportation using LH2 as fuel.

CHAPTER 2

Reverse engineering

The objective of this Master Thesis is to propose a BWB aircraft analogous to the A350-1000 using hydrogen as fuel. In this chapter, the reverse engineering of the original aircraft will be shown, in addition to the analysis of some BWB prototypes.

1 Similar aircraft

The A350-1000 will be analyzed, as well as the NASA's X-49B and the Airbus BWB prototype for commercial aviation.

1.1 A350-1000

The Airbus A350-1000 is the largest variant of the A350 XWB family of aircraft developed by Airbus. It offers enhanced operational performance, increased efficiency, and increased passenger comfort in order to meet the needs of long-haul, high-capacity routes. Among some of its features, it can be distinguished [12]:

- Size and capacity. The A350-1000 has a length of approximately 73.78 meters (242

feet) and a wingspan of 64.75 meters (212 feet). In a typical three-class layout, it has a seating capacity of about 366 passengers. However, a high-density layout of it can hold up to 440 passengers. The cabin offers a width of $5.61\ m$ and includes a typical three-class configuration. The economy class features 18 in-wide seats.

- Range. The impressive range of the A350-1000 is about 8000 nautical miles (14800 kilometers). This enables it to run on lengthy routes, such as intercontinental flights, linking far-off cities all over the world.

Figure 2.1: Picture of an A350-1000 [13].

- Engine. The A350-1000 is powered by Rolls-Royce Trent XWB-97 engines, specifically designed for this aircraft model, which generate a thrust of 97000 lb during take-off. These engines, which are the most potent members of the Trent XWB engine family, give the A350-1000's increased size and performance requirements the necessary thrust.

- Wing design. The A350-1000's advanced aerodynamic wing design is similar to that of other A350 XWB family members. To lessen drag and increase fuel efficiency, it features a moderate sweep angle, laminar flow control, and optimized wingtip devices. Additionally, the wings have a higher aspect ratio, which improves lift-to-drag ratio for better overall performance [14].

- Advanced materials. Modern composite materials, like carbon fiber-reinforced polymer (CFRP), are used in the construction of the A350-1000. More than 50% of the fuselage is constituted by CFRP. The aircraft's operational performance and fuel efficiency are improved by using these lightweight materials, which also help reduce the aircraft's overall weight.

- Fuel Efficiency and Environmental Performance. The A350-1000 boasts impressive fuel efficiency, thanks to its aerodynamic design, advanced engines, and lightweight materials. It consumes approximately 25% less fuel compared to previous generation aircraft in its class. The A350 is an eco-efficient, sustainable clean-sheet aircraft designed to be a quieter, cleaner aircraft delivering 25% less fuel burn and CO2 emissions per seat [15].

In summary, the Airbus A350-1000 is a technologically advanced and efficient aircraft, designed for long-haul travel with increased passenger capacity.

1.2 X-48B

A prototype unmanned aerial vehicle (UAV), known as the X-48B, was created by NASA and Boeing. Its goal was to investigate the aerodynamic and functional properties of an aircraft configuration with a blended wing and body [16].

Figure 2.2: X-48B [17].

The X-48B has a wingspan of $6.4\ m$, weighs $178\ kg$, and is built with composite materials. It is powered by three small turbojet engines and is expected to fly up to $220\ km/h$ and reach an altitude of $3000\ m$. The X-48B is an 8.5% scale version of a $73\ m$ wingspan concept design. The vertical tails were located at the wingtips and the engines at the extreme aft of the aircraft's body. After the X-48B tests, it was seen that BWB aircraft could effectively fulfill the role of heavy-lift transport in military service and long-haul airliner in civilian service.

There are another 2 models of the X-48: X-48A and X-48C. The X-48A was the first prototype of the research with a wingspan of 10.7 meters. However, it was cancelled in the early design stages. The X-48C was an upgraded version of the X-48B, where the vertical stabilizers were reallocated at the sides of the engines, and the fuselage was extended rearward. Both modifications were done to reduce the aircraft's nose profile. It was powered by two (instead of three) JetCat turbojets. It was also designed to study the noise, an important parameter for civilian commercial aircraft. After the X-48C test flights, Boeing and NASA announced new aircraft flight tests to develop a larger BWB demonstrator, capable of transonic flight.

The X-48B program successfully demonstrated the viability of the blended wing body concept for future aircraft designs. The research and data gathered from the X-48B contributed to a greater understanding of the blended wing body configuration and its potential applications in commercial, military, and unmanned aircraft designs.

1.3 Airbus MAVERIC

According to Airbus [18], the development of MAVERIC prototype began in 2017 as part of the AirbusUpNext research program. It was revealed on February 11st 2020, in the Singapore Airshow. Later, on September 21, 2020, Airbus revealed three concepts for the hydrogen-powered Airbus ZEROe, the lartgest of them being a blended wing aircraft based on the MAVERIC.

The Airbus MAVERIC is an experimental blended wing body unmanned aircraft, built as a demonstrator for a possible full-scale BWB airliner. Airbus claims that this design can reduce up to 20% of fuel. It has a wingspan of $3.2\ m$, a length of $2\ m$ and a wing area of $2.25\ m^2$. It is powered by two engines mounted over the rear of the aircraft, with two vertical stabilizers on them.

The development of demonstrators like MAVERIC is enabling Airbus to accelerate understanding of new aircraft configurations and to mature the technology necessary to fly such a radically different aircraft.

Figure 2.3: Airbus MAVERIC [19].

In order to have some reference values of their geometry, these are obtained and shown in Table 2.1. These aircraft consist of three parts: the fuselage wing (or cabin), the main wing, and the joint between these two, which is called 'blending zone'.

Parameter	Airbus Maveric			X-48B		
	Fuselage wing	Blending zone	main wing	Fuselage wing	Blending zone	main wing
$\Lambda_{LE}\,(deg)$	57.9	57.9	30.6	54.3	33.8	33.8
$\Lambda_{TE}\,(deg)$	-12.7	-24.6	13.4	-28.1	-18.6	20
λ	0.539	0.414	0.3114	0.3795	0.5420	0.4151
$S_w\,(m^2)$	1.34	0.448	0.494	5.790	1.306	1.488

Table 2.1: Basic geometrical parameters of Airbus Maveric and X-48B.

2 Mission profile

The mission profile analysed will be the same as the one of the new design. Since these aircraft are built for commercial activities, their mission will be:

- Take-off: the aircraft goes from moving along the ground to fly in the air.
- Climb and acceleration: the engine runs at a certain power in order to reach the cruise altitude at the desired cruise speed.
- Cruise: the aircraft flies at $M = 0.75$ at an altitude of $h = 11500\,m$.
- Descent: the aircraft decreases altitude before landing.
- Landing: final phase of the mission. The aircraft lands in the airport.

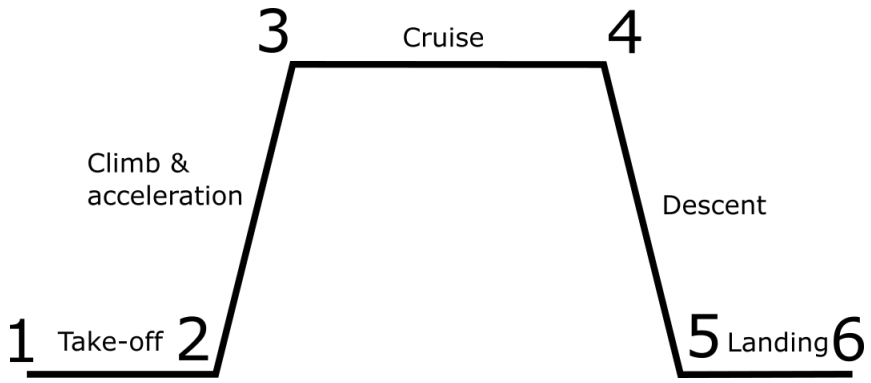

Figure 2.4: Mission profile of the A350-1000.

3 Reverse engineering

Now that the basic data about the A350-1000 is obtained, a reverse engineering process can be performed in order to obtain as much technical and performance information as possible.

During this phase and the design process, both Corke's [20] and Raymer's [21] methodologies will be used.

3.1 Flight conditions

Flight conditions will vary along the whole cruise, since the weight of the aircraft is decreasing along time as fuel is consumed. There is no expendable payload.

As weight decreases, Lift needs also to be decreased in order to maintain a leveled flight. There are three modes of flying an aircraft: variable velocity, variable height and variable angle of attack. As commercial aircraft are flown at maximum speed to reach the destination as soon as possible, and the change in altitude depends on the air traffic controller, this study will be done considering variable angle of attack.

At cruise altitude, $h = 11500\,m$, following the ISA model, the conditions are:

- $z = 11500\,m$
- $a = 295.06\,m/s$
- $T = 216.65\,K$
- $\rho = 0.336\,kg/m^3$
- $\nu = 4.226 \cdot 10^{-5}\,m^2/s$

3.2 Basic geometry

Using CAD software like Fusion360 and sketches of the A350-1000, the basic geometry of the aircraft is obtained. Knowing that it is a Tube and Wing aircraft with a conventional stabilizer, the geometrical data is shown in Figure 2.2.

3.3 Aerodynamics

In this subsection, the aerodynamics of the A350-1000 will be analyzed for the cruise conditions.

The airfoil used in A350-1000 main wing is not public knowledge, but it is known that it uses a supercritical airfoil. For this reason, the study will use the NASA SC(2)-0714 airfoil.

Wing	V-Tail	H-Tail	Fuselage
$S = 464.3\,m^2$	$S = 40.8\,m^2$	$S = 78.1\,m^2$	$l = 67.518\,m$
$b = 64.75\,m$	$b/2 = 8.578\,m$	$b = 18.28\,m$	$d = 6\,m$
$AR = 9.02$	$AR = 7.21$	$AR = 4.27$	$S_{,wet} = 1272.7\,m^2$
$b_{winglet} = 4.075$	$c_{rt} = 6.87\,m$	$c_{rt} = 6\,m$	
$c_{rt} = 11.37\,m$	$c_{tip} = 2.64\,m$	$c_{tip} = 2.55\,m$	
$c_{tip} = 2\,m$	$c_{mac} = 5\,m$	$c_{mac} = 4.5\,m$	
$c_{mac} = 7.78\,m$	$\lambda = 0.384$	$\lambda = 0.424$	
$\lambda = 0.175$	$\Lambda_{c/4} = 39.76°$	$\Lambda_{c/4} = 33.5°$	
$\Lambda_{LE} = 34.35°$			
$\Lambda_{c/2} = 28.1°$			
$\Lambda_{c/4} = 31.33°$			
$\Gamma = 6.71°$			

Table 2.2: A350's geometrical parameters.

Feature	NASA SC(2)-0714
$C_{l_{max}}$	1.75
C_{l_α}	$0.0875\,deg^{-1}$
$\alpha_{stall,2D}$	$15.00\,deg$
α_{0L}	$-5\,deg$
t_{max}	$0.14\,c_w$
x_{max}	$0.37\,c_w$

Table 2.3: NASA SC(2)-0714 2D data.

Its characteristics in 2D can be seen in Table 2.3 [22]. Where t_{max} is the maximum thickness with respect to the chord length and x_{max} the longitudinal position of the maximum thickness with respect to the chord length.

For both horizontal and vertical tails, a symmetrical airfoil is going to be selected. The airfoil selected is the NACA 0012 and its properties shown in Table 2.4 [22].

3D lift-related coefficients

From the airfoil's 2D data, the 3D wing lift-related coefficients can be obtained [20] [21].

Knowing that the Lift equation is:

$$C_L(\alpha) = C_{L\alpha} \cdot \alpha + C_{L0} = C_{L\alpha}(\alpha - \alpha_{0L}) \tag{2.1}$$

Feature	NACA 0012
$C_{l_{max}}$	1.4
C_{l_α}	$0.0933\, deg^{-1}$
$\alpha_{stall,2D}$	$15.00\, deg$
α_{0L}	$0\, deg$
t_{max}	$0.12\, c_w$
x_{max}	$0.3\, c_w$

Table 2.4: NACA 0012 2D data.

The slope of the linear section is obtained as:

$$C_{L_\alpha} = \frac{2\pi\, AR}{2 + \sqrt{4 + (AR\,\beta)^2 \cdot \left[1 + \frac{tan\,(\Lambda_{LE})^2}{\beta^2}\right]}} \tag{2.2}$$

Where the sweep angle Λ_{LE} is in rad and $\beta = \sqrt{1 + M_{eff}^2}$, being $M_{eff} = M_{cr} \cdot cos(\Lambda_{LE})$. And the lift coefficient for $\alpha = 0°$ (C_{L0}) can be obtained as:

$$C_{L_{\alpha=0}} = -C_{L_\alpha} \cdot \alpha_{0L} \tag{2.3}$$

On the other hand, the maximum (3D) lift coefficient C_{Lmax} can be obtained analytically.

According to Raymer:

$$C_{L_{max}} = 0.9\, C_{l_{max}}\, cos\Lambda_{0.25c} \tag{2.4}$$

Knowing $C_{L_{max}}$ and C_{L0}, α_{max} is calculated through:

$$\alpha_{max} = \frac{C_{L_{max}} - C_{L0}}{C_{L_\alpha}} \tag{2.5}$$

The lift coefficient required at cruise conditions is calculated as:

$$C_L = \frac{W \cdot g}{q \cdot S_w} \tag{2.6}$$

The relevant data of the 3D wing coefficients are present in Table 2.5

Estimation of Drag

It is possible to determine the main drag contributions of the aircraft during cruise. As Corke [20] explains, the main wing's drag coefficient can be expressed as:

Parameter	Value
C_{L_α}	$0.0852\ deg^{-1}$
$C_{L_{\alpha=0}}$	0.426
$C_{L_{max}}$	1.345
α_{stall}	$10.77\ deg$

Table 2.5: A350-1000 lift-related coefficients (main wing).

$$C_D = C_{D_0} + C_{D_i} \tag{2.7}$$

where:

- C_{D_0} is the base (zero-lift) drag coefficient.
- $C_{D_i} = k_{ind}\, C_L^2$ represents the induced (due to lift) drag coefficient.

Wing's base Drag. The base drag coefficient C_{D_0} can be estimated with the geometrical parameters. So that:

$$C_{D_{0,w}} = C_f \cdot F \cdot Q \cdot \frac{S_{wet}}{S_w} = 0.00784 \tag{2.8}$$

Where:

- C_f is the skin friction coefficient that depends on the Reynolds number. It is based on the longitudinal development length of the boundary layer and the Mach number. For laminar flow conditions:
$$C_f = \frac{1.328}{\sqrt{Re}} \tag{2.9}$$
For turbulent flow conditions in cruise:
$$C_f = \frac{0.455}{log_{10}(Re)^{2.58}(1 + 0.144M^2)^{0.65}} \tag{2.10}$$
It must be taken into account the $Re_{cut\,off}$. This parameter means that the C_f remains constant above $Re_{cut\,off}$. For subsonic flight:
$$Re_{cut\,off} = 38.21(c/k)^{1.053} \tag{2.11}$$
Where k is the surface finishing and equals $0.17 \cdot 10^{-5}\ ft$ as it corresponds to smooth molded composite.

- The form factor, F, is determined by the airfoil's geometry.:

$$F = \left[1 + \frac{0.6}{(x_{max}/c)} \left(\frac{t_{max}}{c}\right) + 100 \left(\frac{t_{max}}{c}\right)^4\right] \left[1.34\, M^{0.18}\, cos(\Lambda_{c/4})^{0.28}\right] \tag{2.12}$$

- Q is the interference factor. Due to component interference, parasite drag is increased. A low wing can have an interference factor from about $1.1 - 1.4$. In this case:

$$Q = 1.25 \tag{2.13}$$

- S_w and S_{wet} are the wing surface and the wetted wing surface, respectively. Knowing the shape of the airfoil and the wing surface, the wetted surface can be estimated analytically and should be slightly larger than two times the wing surface. For $t_{max}/c > 0.05$:

$$S_{wet} = S_w \left[1.977 + 0.52 \left(\frac{t_{max}}{c}\right)\right] \tag{2.14}$$

Estimation of fuselage drag. The method used for this base drag estimation is the same as the previous one. However, in this instance, it is determined by the fuselage length.The cylinder surface formula is used to obtain the $S_{f,wet}$ because the fuselage has a circular section and is largely uniform (except for the rear portion). The resulting drag force, then, is summed up.

$$C_{D_{0f}} = C_f \cdot F \cdot Q \cdot \frac{S_{f,wet}}{S_w} = 0.00527 \qquad S_{f,wet} = 2\,\pi R_f\, l_f \tag{2.15}$$

Note that this drag coefficient is normalized with the wing surface. With the exception of the form factor (F), every parameter in the expression is computed in the same manner as the base drag calculations for the wing.

- For the friction coefficient (C_f), in this case, the Reynolds number is calculated taking the fuselage length (l_f) as the characteristic length. The interference factor (Q) is equal to 1.
- The form factor is calculated as:

$$F = 1 + \frac{60}{(1/\delta)^3} + \frac{(1/\delta)}{400} \tag{2.16}$$

Where $\delta = d_f/l_f$, the so-called fuselage fineness ratio. It has a fineness ratio of $\delta = 0.08304$.

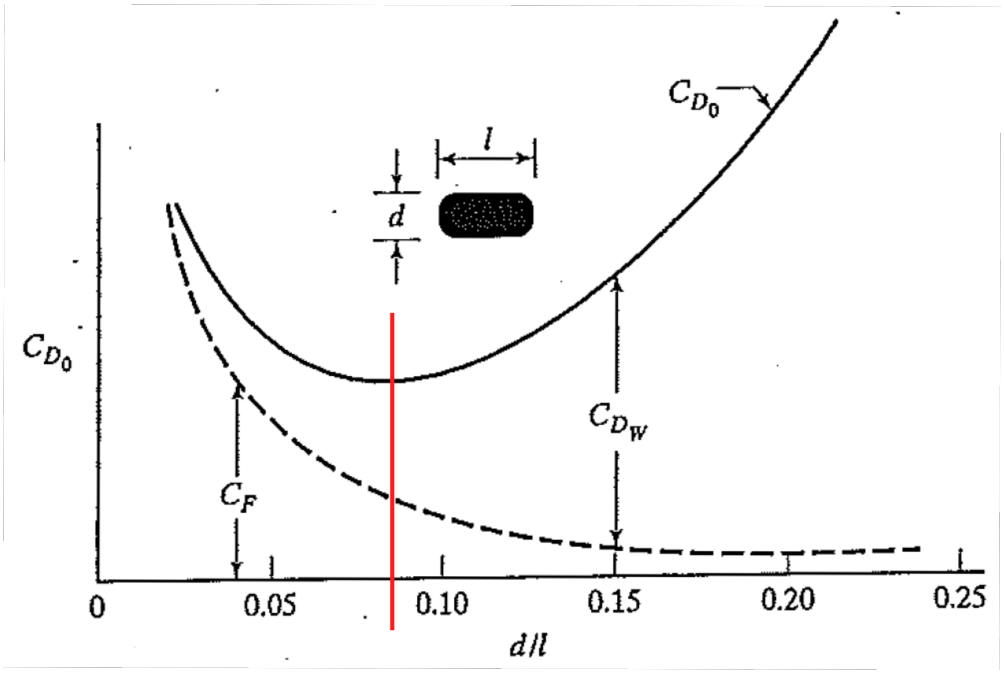

Figure 2.5: Fineness ratio of the fuselage.

In order to calculate the fuselage drag force in cruise conditions:

$$D_f = q\, S_w\, C_{D_f} \tag{2.17}$$

Estimation of vertical and horizontal tail drag. For the horizontal and vertical tails, the exact same procedure as the one used for the main wing's base drag is used, but with the tail's geometry instead. The interference factors are five percent ($Q = 1.05$). So the vertical and horizontal tail's drag contribution to the total drag will be, respectively:

$$\begin{aligned} D_{v\,tail} &= q\, S_w\, C_{D_{vt}} \\ C_{D_{0,vt}} &= 0.000595 \end{aligned} \tag{2.18}$$

$$\begin{aligned} D_{h\,tail} &= q\, S_w\, C_{D_{ht}} \\ C_{D_{0,ht}} &= 0.00118 \end{aligned} \tag{2.19}$$

Where, again, the empennage's drag coefficients are normalized with the main wing's surface.

Engine's drag The engine's drag is calculated the same way as the fuselage's one. In this case, the characteristic length of the Reynolds number will be the length of the engine, and

the form factor is calculated as:

$$\begin{aligned} F &= 1 + 0.35/f_{eng} \\ f_{eng} &= l_{eng}/d_{eng} \end{aligned} \tag{2.20}$$

In this case, the interference factor Q will be 1.5. The drag coefficient will be $C_{D_{0,eng}} = 0.00124$.

Induced drag coefficient. For calculating this coefficient, it is necessary to obtain the induced drag parameter and the (3D) lift coefficient.

The induced drag parameter is calculated as:

$$k_{ind} = \frac{1}{\pi\, AR_{eff}\, e} = 0.0415 \tag{2.21}$$

where the Oswald efficiency has been calculated according to Nita et al. [23] as follows:

$$e = \frac{1}{1.05 + 0.007 \cdot \pi \cdot AR} = 0.8 \tag{2.22}$$

The effect of the winglets is taken into account in the AR_{eff}

$$AR_{eff} = AR(1 + 1.9\, h/b) \tag{2.23}$$

Where h is the endplate height.

Total Drag Coefficient. Once all drag-related coefficients are obtained, the total drag force and total drag coefficient in cruise conditions are:

$$\begin{aligned} C_D &= \sum_i CD_{0,i} + k_{ind}\, C_L^2 = 0.01615 + 0.0415 \cdot C_L^2 \\ D &= q\, S_w\, C_D \end{aligned} \tag{2.24}$$

The contribution of each component of the aircraft in the CD0 is shown in Figure 2.6, where:

- Wing: 48.57%
- Fuselage: 32.67%

- Engines: 7.7%
- Vertical tail: 3.68%
- Horizontal tail: 7.35%

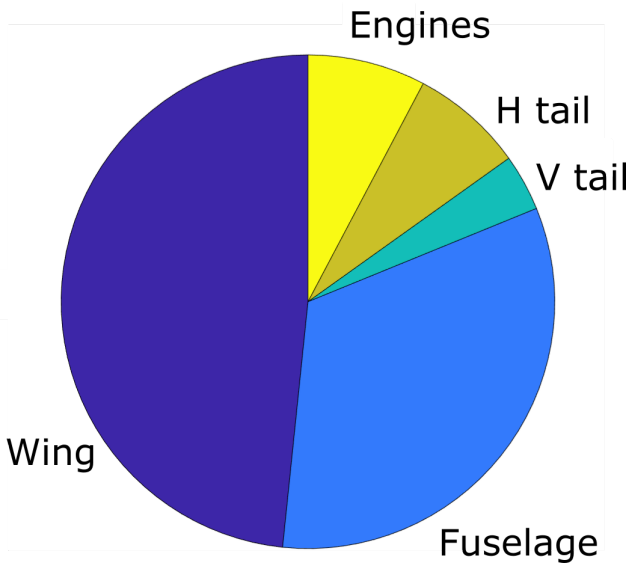

Figure 2.6: Contribution to the C_{D_0} per component.

3.4 Weights

In this analysis, the weight distribution is very important. In particular, it must be known the empty weight, the payload, fuel and maximum take-off weights. The OEW is fixed, and it is assumed that the aircraft carries 369 passengers, with 100 kg associated to each one ($W_{PL} = 36900\ kg$). Then, the fuel weight knowing that the aircraft takes-off at $MTOW$. The weight distribution is summarized in Table 2.6.

Element	Weight [kg]
W_{empty}	155000
W_{PL}	36900
W_{fuel}	127100
$W_{fuel,max}$	128303
$MTOW$	319000
W_{to}	319000

Table 2.6: A350 weight distribution.

Estimation of weight fractions

Weight fractions over the course of the entire mission profile must be computed using the previous weight estimations. Depending on the phase, different amounts of fuel will be used during the flight. Since several parameters depend on the evolution of the aircraft's weight, these changes are significant for the computations.

The mission profile is, as was already mentioned, fairly straightforward and is divided into a few number of phases. The amount of fuel used for any of those phases can be calculated as the final weight divided by the initial weight (in kg). To determine the aircraft performance in terms of endurance and range, the goal is to determine what percentage of the total weight of available fuel is consumed during each of the phases. These percentages are obtained through correlations with historical data [21].

- Take-off. For engine start-up and take-off, Raymer proposes a weight fraction loss of about 3% .
$$\frac{W_2}{W_1} = 0.97 \tag{2.25}$$
- Climb and accelerate. The fuel fraction in this phase is considered to be:
$$\frac{W_3}{W_2} = 1.0065 - 0.0325M = 0.982 \tag{2.26}$$
- Cruise. The aircraft flies at M = 0.75 at an altitude of h = 11500 m. The weight fraction is obtained knowing the rest fractions:
$$\frac{W_4}{W_3} = \frac{\frac{W_6}{W_1}}{\frac{W_2}{W_1}\frac{W_3}{W_2}\frac{W_5}{W_4}\frac{W_6}{W_5}} = 0.642 \tag{2.27}$$
- Descent. The aircraft changes the altitude from the cruise one to the airport one.
$$\frac{W_5}{W_4} = 0.99 \tag{2.28}$$
- Landing and taxi back. The last stage of the flight
$$\frac{W_6}{W_5} = 0.992 \tag{2.29}$$

3.5 Estimation of propulsion system

The A350-1000 is powered by two Rolls-Royce Trent XWB turbofan engines of $375000\ N$ thrust each (SLS). The reference values of this engine are present in Table 2.7.

For the TSFC evolution (Model X [24]), a reference value of Mach number, ambient temperature and specific fuel consumption must be known to know the new TSFC. The evolution of this fuel consumption depends on the Mach number and the temperature.

$$TSFC = TSFC_{ref} \cdot \sqrt{\frac{M \cdot T}{M_{ref} \cdot T_{ref}}} \tag{2.30}$$

The Thrust model used is the Matingly one [24], where knowing the Thrust at SLS (T0) it is possible to know the force produced by the engine at each altitude and velocity.

$$T(M, \sigma) = T0 \cdot \left(0.568 + 0.25(1.2 - M)^3\right) \cdot \sigma^{0.6}$$
$$\sigma = \frac{\rho}{\rho_{SL}} \tag{2.31}$$

Feature	Data
Fuel type	Jet A / Jet A-1
M_{ref}	0.8
z_{ref}	$10668\,m$
$TSFC_{ref}$	$0.494\,1/h$
$T0$	$375000\,N$

Table 2.7: RR Trent XWB's reference values.

3.6 Estimation of performance

Now that all the variables required to determine the aircraft's performance have been estimated, some relevant results can be obtained.

- Wing loading ($L = W \cdot g$):

$$WL = \frac{W \cdot g}{S_w} = \frac{1}{2}\rho V^2 CL \tag{2.32}$$

- Stall speed:

$$V_{stall} = \sqrt{\frac{W \cdot g}{1/2\,\rho\,S_w\,C_{L_{max}}}} \tag{2.33}$$

- Aerodynamic efficiencies:

$$AE_{max} = \frac{1}{2\sqrt{C_{D_0} \cdot k_{ind}}} \qquad AE = C_L/C_D \tag{2.34}$$

- Endurance in hours (Breguet eq.):

$$E = \sum_{i}^{500} \frac{AE_i}{TSFC_i} \cdot ln\left(\frac{W_i}{W_{i+1}}\right) = \mathbf{17.75\ h} \tag{2.35}$$

  Where $TSFC_i$ is in $1/h$

- Range in kilometers (Breguet eq.):

$$R = \sum_{i}^{500} E_i \cdot V_i \cdot \frac{3600}{1000} = \mathbf{14145\ km} \tag{2.36}$$

  Where V_i is in m/s

According to the results above, the obtained range is sufficiently close to what was found in the literature.

In order to facilitate understanding, the following parameter evolutions during cruise flight will be plotted:

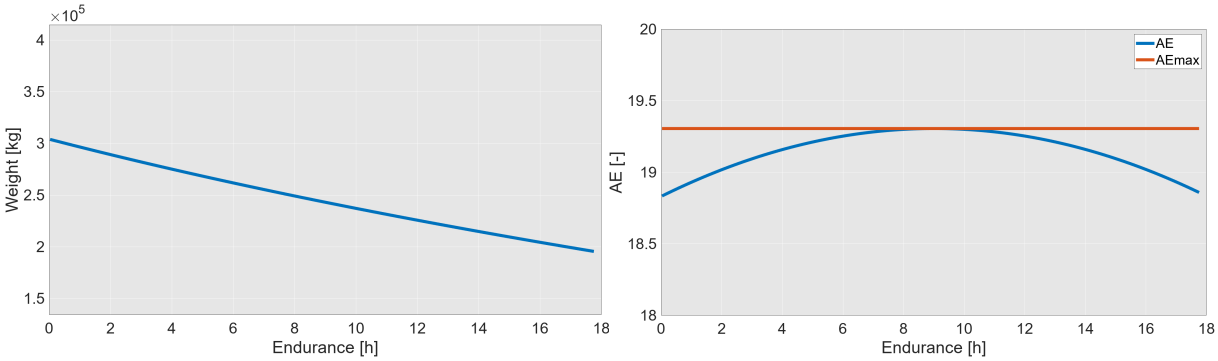

(a) Original Weight vs Endurance evolution. **(b)** Aerodynamic evolution in cruise.

Figure 2.7: Reverse engineering parameter evolutions (I).

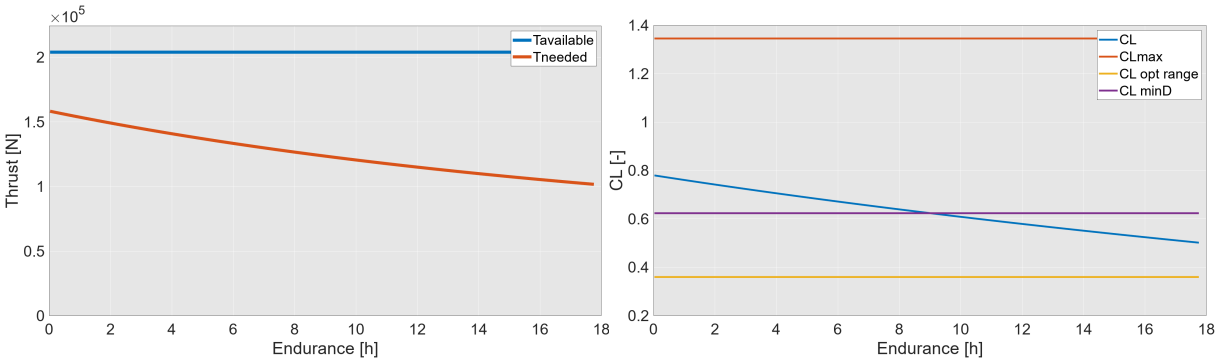

(a) Thrust needed in cruise. **(b)** Lift coefficient evolution.

Figure 2.8: Reverse engineering parameter evolutions (II).

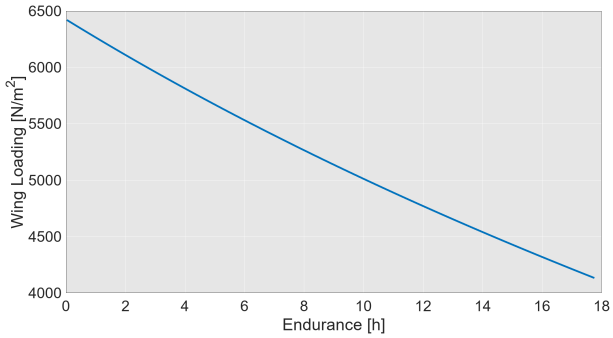

(a) Wing loading evolution

Figure 2.9: Reverse engineering parameter evolutions (III).

In all of the figures above, a decreasing tendency in time/range can be seen because of the fuel weight loss.

In Figure 2.7b, the maximum aerodynamic efficiency is reached at mid cruise. Its value is $AE_{max} = 19.31$. This point corresponds to the one where $C_L = C_{L_{minD}}$ After that, this efficiency is reduced as C_L is also reduced.

Figure 2.8a shows the required thrust (also known as Drag) required for levelled flight, and the force produced by the engines. At the start of the cruise, these two forces are close, but during cruise the required thrust is reduced, as weight also does. This produces a decrease in C_L, which means a decrease in the induced drag and the total drag. The slope seems linear, but it is not at all as the function of the Drag is quadratic (in function of C_L). The TSFC is maintained constant, as M or height doesn't change, and has a value of $0.4763\ 1/h$

In Figure 2.8b can be seen the lift coefficient evolution. The C_L required in cruise is always lower than the maximum C_L. It starts with a value of $C_L = 0.779$ and ends with $C_L = 0.501$. The value for minimum drag is achieved at mid cruise, but the one for maximum range is

never achieved as it is too low.

CHAPTER 3

The new BWB aircraft

1 Initial sizing

For the design of the new aircraft, the initial sizing consists of two blocks: 'Weight estimation' and 'Initial aerodynamics'. In Weight estimation, an initial approach of the fuel weight and empty weight are obtained. Then the geometry of the aircraft is obtained based on similar aircraft and knowledge of aerodynamics, and finally it is analyzed in Aerodynamics block.

1.1 Weight estimation

In this section the different weights of the aircraft are obtained:

Fuel weight

To estimate the weight of fuel needed, weight fractions of each segment are calculated as in the reverse engineering. However, the effect of the use of hydrogen must be taken into account. For this reason the consumption of this fuel will be 36% the one of Jet-A, as demonstrated in the section 2.

- Take-off. .

$$\frac{W_2}{W_1} = 1 - 0.36 \cdot 0.03 = 0.9892 \tag{3.1}$$

- Climb and accelerate.

$$\frac{W_3}{W_2} = 1.0065 - 0.36 \cdot 0.0325M = 0.9977 \tag{3.2}$$

- Cruise. In this part the Breguet's equation will be used, where R is the design range, V is the velocity and AE the aerodynamic efficiency. As they are design parameters, it is chosen the AE to be 20 (as it is very close to the A350-1000), the velocity is the one for $M = 0.75$, and range will be $13000\,km$. The TSFC is the 36% the one of RR Trent XWB turbofan using kerosene. It must be taken into account that the aerodynamic efficiency will be higher than the A350-1000 one, but as an initial approach it will be valid.

$$\frac{W_4}{W_3} = \exp\frac{-R \cdot TSFC}{V \cdot AE} = 0.8694 \tag{3.3}$$

- Descent.

$$\frac{W_5}{W_4} = 1 - (1 - 0.99) \cdot 0.36 = 0.9964 \tag{3.4}$$

- Landing and taxi back.

$$\frac{W_6}{W_5} = 1 - (1 - 0.992) \cdot 0.36 = 0.99712 \tag{3.5}$$

Knowing all these fraction, the ratio between the final and initial weight is obtained (being $W_1 = W_{to}$):

$$\frac{W_6}{W_1} = \frac{W_2}{W_1} \cdot \frac{W_3}{W_2} \cdot \frac{W_5}{W_3} \cdot \frac{W_6}{W_5} = 0.8525 \tag{3.6}$$

Using this value, it is possible to obtain the fuel fraction:

$$\frac{W_{fuel}}{W_{to}} = 1 - \frac{W_6}{W_1} = 0.14746 \tag{3.7}$$

Empty Weight

The empty weight is calculated using the correlation given by Raymer [21] for jet transport aircraft. It has the following shape:

$$\frac{W_{empty}}{W_{to}} = A \cdot W_{to}^C \cdot K_{vs} \tag{3.8}$$

Where $A = 0.97$, $C = -0.06$ and $K_{vs} = 1$. As this correlation is used with aircraft that that use kerosene as fuel where tanks are mounted in the wings, this empty weight fraction doesn't

take into account the weight of the tanks. Therefore, the weight of the tanks is obtained using the fuel weight and the Gravimetric index:

$$W_{tanks} = W_{fuel}\left(\frac{1}{GI} - 1\right) \tag{3.9}$$

The mission of this aircraft is to carry 300 passengers in a long flight. It is assumed that each passenger has 100 kg associated, and doing so the weight of the payload is calculated. For the crew weight, it is taken into account the two pilots and six flight assistants. Knowing the fraction of fuel, the crew and payload weights, the take-off weight can be estimated according to the following formula:

$$W_{to} = \frac{W_{PL} + W_{crew}}{1 - \frac{W_{fuel\ system}}{W_{to}} - \frac{W_{empty}}{W_{to}}} \tag{3.10}$$

This is accomplished through an iterative process. The empty weight fraction is first calculated using an estimated initial take-off weight. The latter involves calculating the second take-off weight, which results in a different empty weight value. This is carried out until the empty weight and take-off weight converge. The obtained results are:

- Take-off weight: $W_{to} = W_1 = 257973\ kg$
- Empty weight (without tanks): $W_{empty} = 118482\ kg$
- Empty weight (with tanks): $W'_{empty} = 189131\ kg$
- Fuel weight: $W_{fuel} = 38042\ kg$
- Volume of fuel: $V_{fuel} = 535.8\ m^3$
- Tanks weight: $W_{tanks} = 70649\ kg$
- Fuel system weight = $W_{fuel\ system} = W_{fuel} + W_{tanks} = 108691\ kg$
- Payload weight: $W_{PL} = 300 \cdot 100\ kg = 30000\ kg$
- Crew weight: $W_{crew} = 8 \cdot 100\ kg = 800\ kg$
- Weight at the start of the cruise: $W_{cr,start} = 254606\ kg$
- Weight at the end of the cruise: $W_{cr,end} = 221363\ kg$
- Landing weight: $W_{land} = 219931\ kg$

1.2 Geometry and aerodynamics

The design of the new aircraft will be based on similar ones and in some aerodynamic considerations. The fuselage wing design will be driven by capacity factors. The airplane must be able to carry 300 passengers, and that means that there has to be enough space for all the seats. Added to this, liquid hydrogen has a very low density, which implies that to store it a lot of space will be required. This part will be as width as possible, so that there's no space lost at the rear part of the airfoil. By doing this, it is possible to reduce the wetted surface and the base drag. Knowing similar aircraft geometry, the wing is designed to have similar taper ratio (λ) and $\frac{Length}{b/2}$ as the X-48B.

Parameter	Fuselage wing	Main wing
$\Lambda_{LE}\,(deg)$	55	31
$\Lambda_{TE}\,(deg)$	-22.7	12.2
λ	0.2941	0.294
$c_r\,(m)$	34	10
$c_{tip}\,(m)$	10	2.94
$S_w\,(m^2)$	572	237.45
$\%\,S_w$	70.66	29.33

Table 3.1: Geometry parameters of BWB.

The wingspan is obtained using similar $\frac{Length}{b/2}$. This parameter for the X-48B is 1.12 , and for the Maveric is 1.24. The value of this parameter for the initial prototype will be 1.08. With respect to the taper ratio, the Maveric aircraft has a $\lambda_{global} = 0.0694$ and the X-49B a $\lambda_{global} = 0.0853$, so the designed aircraft will have $\lambda_{global} = 0.0864$. This aircraft has an AR of 4.85, which is between the one of the X48B (4.93) and the Maveric (4.55). The sweep parameters are obtained the same way: using the values of similar aircraft.

The airfoil used in this design in the fuselage wing is the NACA 4418 airfoil. It has been chosen this one because Boeing study [25] suggests that the minimum $\frac{t}{c}$ of a BWB should be 0.17 in order to allocate passengers, cargo, and systems within the wing itself. This value is tipically associated with transonic airfoils. In addition, to help with this allocation, the maximum thickness should be at the middle of the chord. So NACA 4418 has the maximum thickness at 40% of it. Its characteristics in 2D can be seen in Table 3.2 [22].

On the other hand, three different geometries were studied. The first one had a distinguished blending part. The second one had a small blending part and the third one doesn't have. In Figure 3.1, the projected area of these prototypes can be seen. They were analyzed aerodynamically with *Tornado VLM*, and the result was that the most efficient geometry was the third one, being able to reach a maximum aerodynamic efficiency of 23.04 . For this

Feature	NACA 4418
$C_{l_{max}}$	1.55
C_{l_α}	$0.1\ deg^{-1}$
$\alpha_{stall,2D}$	$15.00\ deg$
α_{0L}	$-4\ deg$
t_{max}	$0.18\ c_w$
x_{max}	$0.4\ c_w$

Table 3.2: NACA 4418 2D data.

reason, the new design will be based on this geometry.

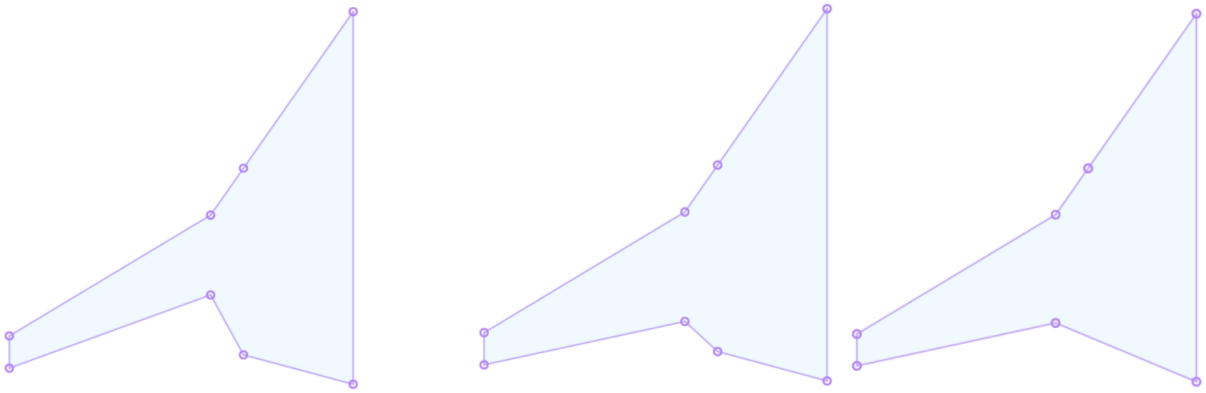

(a) BWB 1's planform. **(b)** BWB 2's planform. **(c)** BWB 3's planform.

Figure 3.1: Comparision of three blending parts.

	BWB 1	BWB 2	BWB 3
K	0.0723327	0.070839	0.068447
CD0	0.0068309	0.0068198	0.006876
Sw	771.032	828.958	809.45
AEmax	22.49	22.74	23.04
Endurance	18.05	18.46	18.69
Range	14383.98	14708.22	14897.71

Table 3.3: Data of the three prototypes.

Table 3.3 shows how do the aerodynamic coefficients change when the blending zone is removed. This is due to there are less lift induced drag at the edge of the fuselage wing.

2 Aerodynamics

An aircraft's conceptual design is the first stage of the design process, during which the fundamental characteristics and overall design of the aircraft are chosen. The process entails developing a general concept or idea for the aircraft, which will include information on the aircraft's design, weight, propulsion system, and intended use. Later design stages can conduct in-depth research and make improvements thanks to the conceptual design stage's foundational work.

Aerodynamics are estimated during this stage with a relatively low computational cost and a moderate degree of precision. So it will be more thoroughly examined in later design stages. In particular, the methodology of Corke and Raymer takes into account empirical models for calculating the aerodynamic parameters. However, these are limited to Tube and Wing configuration aircraft, requiring the use of a different approach.

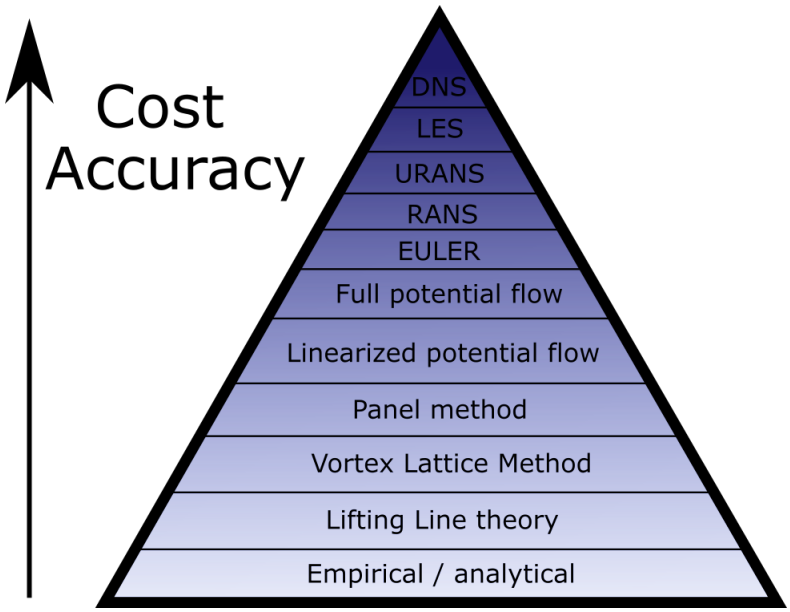

Figure 3.2: The different fidelity levels for aerodynamics solvers.

Figure 3.2 shows the different methods available for the aerodynamics solving, and their fidelity and cost. Due to the geometry complexity of a BWB aircraft, in this thesis a Vortex Lattice Method will be used.

2.1 TORNADO VLM

The Vortex Lattice Method is a numerical method to analyze the dynamics of fluids. VLM models a surface on aircraft as infinite vortices to estimate the lift curve slope, induced drag,

and force distribution. It has been applied to the estimation of aerodynamic properties of lifting surfaces and even full airplanes. The VLM is an extension of Prandtl's lifting line theory that is applicable to a broader range of lifting surfaces including swept and low aspect ratio wings. In this research, a VLM will be used to estimate the value of aerodynamic parameters such as C_L, C_D, C_M, and lift-to-drag ratio. It is assumed that the fluid flows as an incompressible and inviscid fluid, and the thickness effect and viscosity are neglected.

The Vortex Lattice Method represents the aircraft's lifting surfaces, such as wings and tail, as a lattice of vortex filaments. Each vortex filament corresponds to a small segment of the wing and induces a flow field that affects neighboring vortex filaments. The collective behavior of these vortices determines the aerodynamic forces and moments experienced by the aircraft. In this case, *Tornado VLM* will be used to solve the aerodynamics of the Blended Wing Body aircraft. Figure 3.3 shows an example of how the lattice is created in *Tornado VLM*

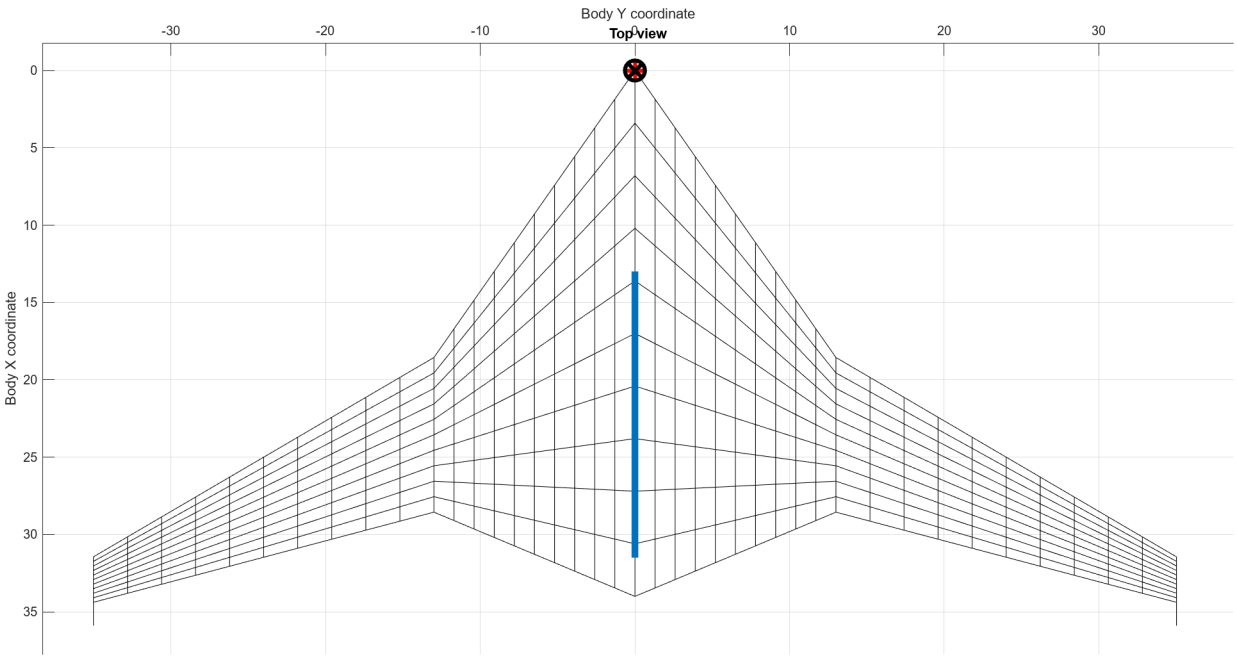

Figure 3.3: Lattice in Tornado VLM.

Tornado VLM is built in Matlab and can be used to configure a variety of aircraft, from simple to complex, and it offers helpful insights into the aerodynamic behavior of the aircraft. Concretely, *Tornado VLM* will allow to obtain the lift coefficient and induced drag, and has an option to calculate the C_{D_0}.

2.2 Sensitivity analysis

The main wing's geometry will be optimized using a sensitivity analysis. The performance is compared and examined by altering some parameters by a particular percentage. With the

significance of the relative variation, a parameter's sensitivity will rise. By doing this, the dominant parameters are identified, making it simple to create the new design.

The results in Table 3.4 were obtained. While change in taper ratio does not produce a significant effect in aerodynamic efficiency, the change in wingspan does.

	BWB3_1	**BWB3_2**	**BWB3_3**	**BWB3_4**
	$\mathbf{b_{mainwing} + 15\%}$	$\mathbf{b_{mainwing} - 15\%}$	$\lambda_{\mathbf{mainwing}} + \mathbf{15\%}$	$\lambda_{\mathbf{mainwing}} - \mathbf{15\%}$
$b_{mainwing}\ (m)$	21.1	15.6	18.35	18.35
$\lambda_{mainwing}\ (-)$	0.294	0.294	0.338	0.25
$\lambda_{total}\ (-)$	0.0864	0.0864	0.0994	0.0735
$C_{D_0}\ (-)$	0.006928	0.00682	0.006876	0.006876
$k_{ind}\ (-)$	0.06146	0.07738	0.0687	0.06834
$S_w\ (m^2)$	845	774	818	801
$AE_{max}\ (-)$	24.23	21.76	23	23
$Endurance\ (h)$	19.75	17.36	18.68	18.69
$Range\ (km)$	15737	13837	14882	14895

Table 3.4: Results of the sensitivity analysis.

To increase the aerodynamic efficiency the wingspan needs to be increased. For this reason, the final design will be increased $+20\%$. It is not increased anymore because the increase of the wingspan leads to an increase of weight and the bending moment. With this, the new geometry parameters will be:

	Fuselage wing	**Main wing**
$\Lambda_{c/4}(deg)$	44	26.8
$\lambda\ (-)$	0.2941	0.294
$c_{rt}\ (m)$	34	10
$c_{tip}\ (m)$	10	2.94
$S_w\ (m^2)$	572	284.93
$\%S_w\ (-)$	66.75	33.25
$w/2\ local\ (m)$	13	22.02

Table 3.5: Geometry of the final aircraft.

This configuration will have:

- $C_{D_0} = 0.0069441$
- $k_{ind} = 0.059344276$
- $S_w = 856.93\, m^2$

- $AE_{max} = 24.63$
- $AR = 5.72$
- $Endurance = 20.06\,h$

3 Refined weights

Previously the empty weight (also known as structural factor) was estimated by calculating its fraction with respect to the take-off weight through statistical methods. However, as the estimation of weights in the conceptual design is a critical part of the design process, more sophisticated weights methods are applied to obtain the weight of the various components of the aircraft, and their sum results in the total empty weight. This new technique uses detailed statistical equations for the various components. It is sufficiently detailed to provide a credible estimate of the weights of the major component groups. The equations will be mainly based in Raymer's correlations [21].

- Wing weight. In this case the equation given by Ikeda et al. [26] will be used. This one comes from analyzing different modern aircraft.

$$W_{wing} = 3.8297 \cdot S_{wing}^{1.0156} \tag{3.11}$$

- Cabin weight. As the cabin is different, Raymer's correlations can't be used. Instead, it will be used a mass prediction method developed by NASA for BWB aircraft. It depends on the W_{to} and area of the cabin. [27]. As it was created for a 450 passenger aircraft, the equation must be redefined with a scale factor for a 300 passenger aircraft. [26]

$$W_{cabin} = \frac{5.698865}{450} \cdot n_{pax} \cdot 0.316422 \cdot W_{to}^{0.16655} \cdot S_{cabin}^{1.06116} \tag{3.12}$$

- Aft centre-body. The weight of the aft centerbody [27] was estimated by treating it as a horizontal tail, and modifying the horizontal tail weight equation to include a factor for the number of engines supported by the centerbody if the aircraft has distributed propulsion or boundary layer ingestion arrangement. The weight of the aft centerbody is then

$$W_{aft} = (1 + 0.05 \cdot N_{en}) \cdot 0.53 \cdot S_{aft} \cdot W_{to}^{0.2} \cdot (\lambda_{aft} + 0.5) \tag{3.13}$$

- Vertical tail.

$$W_{v\,tail} = 0.0026 \cdot (1 + Ht/Hv)^{0.225} \cdot W_{dg}^{0.556} \cdot N_z^{0.536} \cdot L_t^{-0.5} \cdot S_{vt}^{0.5} \cdot K_z^{0.875} \cdot cos(\Lambda_{vt})^{-1} \cdot A_v^{0.35} \cdot (t/c)_{root}^{-0.5} \tag{3.14}$$

- Landing gear.

$$W_{main\,lg} = 0.0106 K_{mp} W_l^{0.888} N_l^{0.25} L_m^{0.4} N_{mw}^{-0.321} N_{mss}^{-0.5} V_{stall}^{0.1} \tag{3.15}$$

$$W_{nose\,lg} = 0.032 K_{np} W_l^{0.646} N_l^{0.2} L_n^{0.5} N_{nw}^{0.45} \tag{3.16}$$

- Engine controls.

$$W_{engine\,controls} = 5 N_{en} + 0.8 L_{ec} \tag{3.17}$$

- Starter (pneumatic)

$$W_{starter} = 49.19 \left(\frac{N_{en} W_{en}}{1000} \right)^{0.541} \tag{3.18}$$

- Flight controls.

$$W_{flight\,controls} = 145.9 N_f^{0.554} (1 + N_m/N_f)^{-1} S_{cs}^{0.2} (I_y \cdot 10^{-6})^{0.07} \tag{3.19}$$

- APU. [28]

$$W_{APU} = 3.175 N_{seats} \tag{3.20}$$

- Instruments

$$W_{instruments} = 4.509 K_r K_{tp} N_c^{0.541} N_{en} (L_f + B_w)^{0.5} \tag{3.21}$$

- Hydraulics.

$$W_{hydraulics} = 0.2673 N_f (L_f + B_w) \tag{3.22}$$

- Electrical system.

$$W_{electrical} = 7.291 R_{kva}^{0.782} L_a^{0.346} N_{gen}^{0.1} \tag{3.23}$$

- Avionics.

$$W_{avionics} = 1.73 W_{uav}^{0.983} \tag{3.24}$$

- Furnishing

$$W_{furnishing} = 0.0577 N_c^{0.1} W_c^{0.393} S_f^{0.75} \tag{3.25}$$

- Air conditioning.

$$W_{air\,conditioning} = 62.36 N_p^{0.25} (V_{pr}/1000)^{0.604} W_{uav}^{0.1} \tag{3.26}$$

- Anti-ice.

$$W_{anti-ice} = 0.002 W_{dg} \tag{3.27}$$

- Handling gear.

$$W_{handling\,gear} = 3 \cdot 10^{-4} W_{dg} \tag{3.28}$$

The meaning of each variable can be found in "*Aircraft design: A conceptual approach*"[21] from Raymer and "*A Sizing Methodology for the Conceptual Design of Blended-Wing-Body Transports*"[27] from Kevin R Bradley. The results are:

- Empty weight (without tanks): $W_{empty} = 89890\,kg$
- Empty weight (with tanks): $W'_{empty} = 147008\,kg$
- Tanks weight: $W_{tanks} = 57118\,kg$
- Structural factor (without tanks): $s = 0.431$
- Fuel weight: $W_{fuel} = 30755\,kg$
- Take-off weight: $W_{to} = 208564\,kg$

3.1 Center of gravity

The center of gravity is one of the most important points in an aircraft. Manufacturers calculate the influence of every mass that is placed on the plane, including every last screw. This is because this point affects flight stability, controllability, takeoff and landing rotation, operational flexibility, etc. Calculating the center of gravity is a simple process, it is enough to know the mass of each element and its longitudinal position such that:

$$x_{CoG} = \frac{\sum_i^N xCOG_i \cdot W_i}{\sum_i^N W_i} \tag{3.29}$$

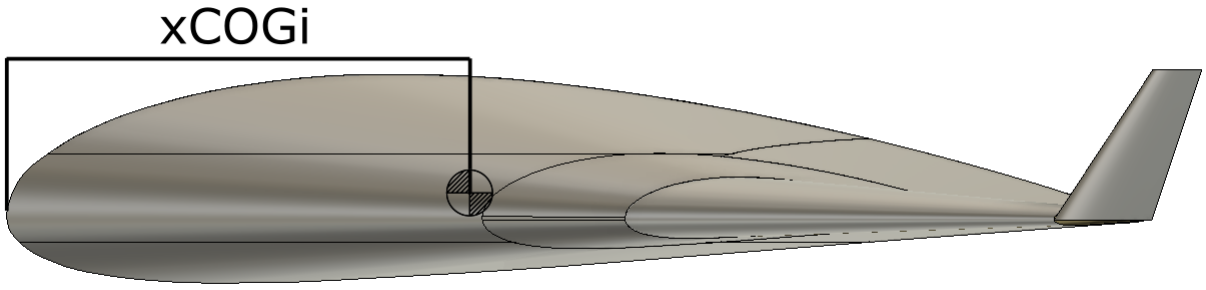

Figure 3.4: Diagram for the calculation of CoG.

Two cases will be analyzed: one in which the plane is loaded with all the fuel, and another in which it is empty. Results are:

- Position of the center of gravity with full fuel: $x_{cog} = 19.47\,m$
- Position of the center of gravity with no fuel: $x_{cog} = 19.28\,m$

4 Engine selection

The next step in the design of the new aircraft is to calculate the Thrust-to-weight ratio. This value will allow to know the required thrust to fly at cruise conditions. To know how the thrust of a turbofan changes with altitude and speed, the *Aerospatiale model* [24] was chosen. Being $\sigma = \rho/\rho_{SL}$:

$$T(M, \sigma) = T0 \cdot [0.568 + 0.25 \cdot (1.2 - M)^3 \cdot \sigma^{0.6}] \tag{3.30}$$

The thrust-to-weight ratio is calculated at the start of cruise, as it is in this moment where the weight of the aircraft is maximum (for all the cruise period). For these calculations, **weight units are in Newton**. Knowing that $W = W_{cr,start} \cdot g$ (in Newtons):

$$\frac{T_{cr}}{W_{cr}} = \frac{C_{D_0} + k_{ind}\left(\frac{W/S_w}{q_{cr}}\right)^2}{\frac{W/S_w}{q}} = 0.0412 \tag{3.31}$$

This value needs to be converted into take-off conditions. Note that $T_{SLS} = T(0,1) = T0$ and $T_{cr} = T(M_{cr}, \sigma_{cr})$ at the beginning of the cruise. Thus, all three fractions at the right side of the following expression are known:

$$\frac{T_{SLS}}{W_{to}} = \frac{T_{cr}}{W_{cr}} \cdot \frac{W_{cr}}{W_{to}} \cdot \frac{T(0,1)}{T(V_{cr}/a_{cr}, \sigma_{cr})} = 0.14966 \tag{3.32}$$

Resulting that the thrust required for the engine at sea level static (SLS) conditions is:

$$T_{SLS} = \frac{T_{SLS}}{W_{to}} \cdot W_{to} = 306208\ N \tag{3.33}$$

The engine is selected from an engine database [7] . As there will be two engines, the engine will be selected to give half of the required thrust. The proposed engine engine will be the PW2337. Its performance parameters are:

- Thrust at Sea Level Static: $T_{SLS} = 162804\ N$
- Thrust-specific fuel consumption: $TSFC_{SLS} = 9.489 \cdot 10^{-6}\ kg/(N\ s)$

However, when calculating the take-off distance in section 6 , this distance is $3390\ m$, large for a height of 500 m. For this reason, a more powerful engine is selected, and is the CF6-80C2B2 . Its performance parameters are:

- Thrust at Sea Level Static: $T_{SLS} = 229483\ N$
- Thrust-specific fuel consumption: $TSFC_{SLS} = 9.0074 \cdot 10^{-6}\ kg/(N\ s)$
- Length: $L_{engine} = 4.2738\ m$
- Diameter: $D_{engine} = 2.6916\ m$
- Weight: $W_{engine} = 4386.2\ kg$

With this new engine, the take-off distance is $2484\ m$, which is an adequate value. However, there will be a little of excess in thrust at the cruise. It will be placed at 3 m from the start of the main wing. It produces an increase in the C_{D_0} of 0.0003887 at cruise conditions. The $TSFC$ at cruise conditions will be $0.199\ 1/h$.

5 Vertical tails

The vertical tails will be placed at the tip of the wing, what commonly is known as winglets. These tails are designed to counteract the moment generated by an engine in situations where one of these fails. The force diagram is shown in Figure 3.5 . So the equilibrium of momentums

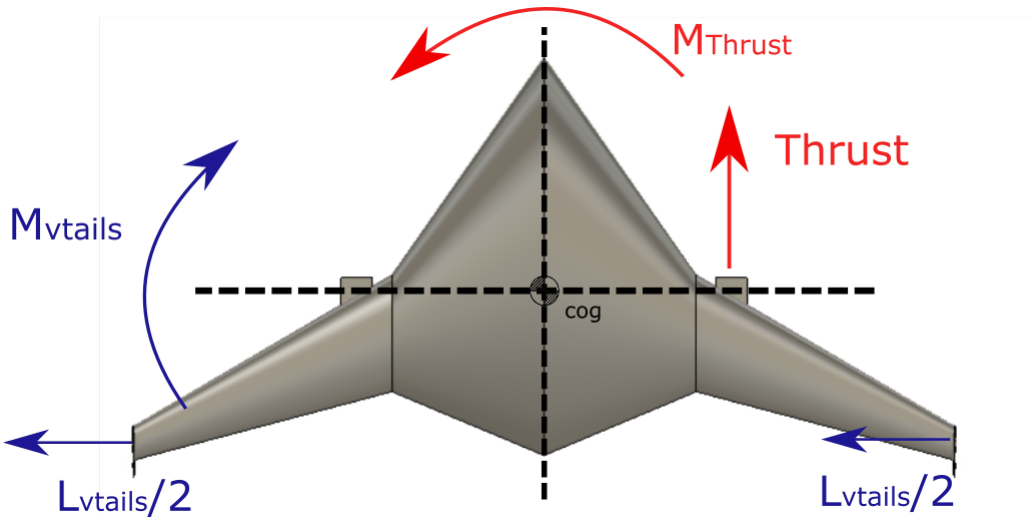

Figure 3.5: Force and moment diagram.

will be:

$$\begin{aligned} M_{v\,tails} = L_{v\,tails} \cdot x_{v\,tails} = M_{engine} = Thrust \cdot y_{engine} \\ L_{v\,tails} = \frac{M_{engine}}{x_{v\,tails}} = \frac{1}{2}\rho V^2 S_t C_L \\ S_{t,required} = \frac{M_{engine}/x_{v\,tails}}{\frac{1}{2}\rho V^2 C_L} \end{aligned} \tag{3.34}$$

The vertical tails are built with the symmetric airfoil NACA 0012 (the same as in the reverse engineering) and produce the lift force through the the deflection of a plain flap. It follows the following expression:

$$C_L = \frac{\partial C_L}{\partial \delta_f} \cdot \delta_f \tag{3.35}$$

Where $\frac{\partial C_L}{\partial \delta_f}$ is the increase in lift generated by the deflection and δ_f is the angle of the plain flap in radians.

The first term is obtained through correlations [29]:

$$\frac{\partial C_L}{\partial \delta_f} = x_1 \cdot x_2 \cdot x_3 \cdot x_4 \tag{3.36}$$

Where:

- $x_1 = \frac{\partial C_{l,2D}}{\partial \delta_f}$
- $x_2 = \frac{C_{L_{\alpha,3D}}}{C_{l_{\alpha,2D}}}$
- $x_3 = K_c \left[\frac{c_{flap}}{c_w ing}, AR\right]$
- $x_4 = K_b \left[\lambda, (\eta_0 - \eta_i)\right]$

The first term (x_1) is:

$$\begin{aligned} \frac{\partial C_{L_{2D}}}{\partial \delta_f} &= 2\pi \left(1 - \frac{\theta_f - sin\theta_f}{\pi}\right) \\ \theta_f &= acos\left[1 - 2\left(1 - \frac{c_f}{c_{tail}}\right)\right] \end{aligned} \tag{3.37}$$

The second term (x_2) is the ratio between the increase in lift with the angle of attack in 3D and 2D. The 3D one is obtained through the Equation 2.2 and the 2D one is 2π. The third and the fourth (x_3, x_4) are obtained through graphical methods present in the report mentioned before [29].

The results are:

- $x_1 = \frac{\partial C_{L,2D}}{\partial \delta_f} = 4.151$
- $x_2 = 0.435$

- $x_3 = 1.35$
- $x_4 = 0.8$
- $\delta_f = 15°$
- $CL_{\alpha,3D} = 2.7368$
- $C_L = 0.511$
- $S_{t,required} = 18.45\, m^2$

The A350-1000 has a vertical tail with a sweep angle at quarter cord ($\Lambda_{c/4}$) of 39º and a taper ratio λ of 0.384 . This values are changed for the Blended Wing Body aircraft design so that the height of these tails is smaller for a given surface. The new taper ratio λ is 0.5 and the sweep angle ($\Lambda_{c/4}$) will be 30º. With this, the new geometry will have a height of $4.5\, m$ and a surface of $9.923\, m^2$.

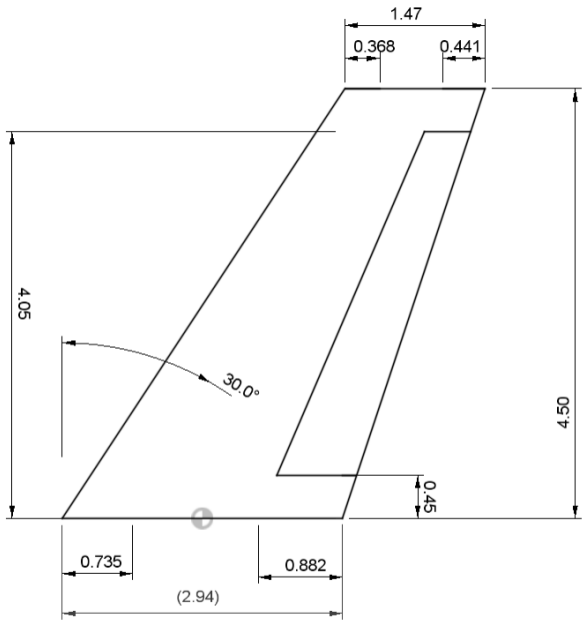

Figure 3.6: Construction sketch of the vertical tail.

Some features of this vertical tail are:

- The deflection of the trailing edge corresponds to 30% of the chord: $\frac{c_F}{c} = 0.3$
- The flap is present in 80% of the span: from $0.1\, b$ to $0.9\, b$.

The addition of the vertical tails at the tip of the main wing has different effects on the aerodynamics. On one hand, the skin friction drag increases due to the increase in wetted surface. On the other hand, the induced drag reduces as this tails act as winglets. To sum up, this effects are:

- $\Delta C_{D_0} = 0.00018111$
- $\Delta k_{ind} = -0.004390907$

The final aerodynamic parameters taking into account the main structure, engines and vertical tails are:

- $C_{D_0} = 0.007513$
- $k_{ind} = 0.05495$

It must be taken into account that the deflection δ_F of a plain flap generates a camber increase that also produces a moment about the aerodynamic center of the tail. However, it is not considered, since it is small compared to the moment that the flap lift generates around the aircraft center of gravity CoG.

5.1 Horizontal tails

Blended Wing Body is a configuration with no horizontal tail. This kind of configuration have short moment arms for pitch and directional control, and, therefore, multiple, large, rapidly moving control surfaces are required. Trailing-edge devices are called on to perform a host of duties, including basic trim, control, pitch stability augmentation, and wing load alleviation. The rear fuselage of the aircraft will be equipped with a tail control surface for pitch control. The rear edge of the wing has two sets of elevons: the outboard elevons are mainly used for roll control, whereas the inboard elevons are used for secondary pitch and roll control (Figure 3.7). Due to their complexity, these surfaces will have to be designed in later phases of the aircraft design.

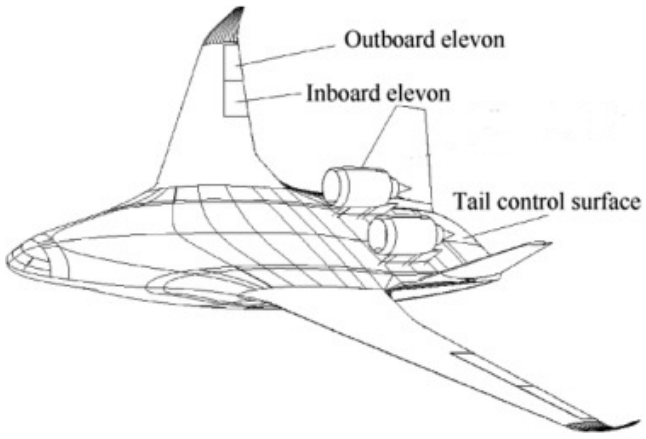

Figure 3.7: Control surfaces for pitch and roll.

6 Take-off and landing distances

Knowing that the typical length of a runway is between 2.4 km and 4 km [30], the engine is selected to give a take-off distance of 2.5 km at 500 m height. In order to compute the performance at low velocity and height phases, aerodynamics are calculated again, this time for a height of 500 m and a velocity of 50 m/s. The results are:

- $C_{D_0} = 0.006418894$
- $k_{ind} = 0.055088307$

6.1 Take-off distance

The take-off distance is divided in four parts: ground roll, rotation, transition and climb.

Ground roll

The aircraft acceleration is expressed as:

$$a = \frac{g}{W}\left[T - D - \mu(W - L)\right] = g\left[\left(\frac{T}{W} - \mu\right) + \frac{\rho}{2W/S_w}(-C_{D_0} - k_{ind}\, C_L^2 + \mu C_L)V^2\right] \tag{3.38}$$

The ground-roll distance is determined by integrating velocity divided by acceleration:

$$S_{Groll} = \int_{Vi}^{Vf} \frac{V}{a} dV = \frac{1}{2}\int_{Vi}^{Vf} \frac{1}{a} d(V^2) \tag{3.39}$$

Where $V_f = 1.1\, V_{stall}$ and $V_i = 0$. This equation is integrated with respect to the terms K_T and K_A. K_T contains the thrust terms and K_A the aerodynamic ones.

$$S_{Groll} = \frac{1}{2g}\int_{Vi}^{Vf} \frac{d(V^2)}{K_T + K_A V^2} = \left(\frac{1}{2gK_A}\right) ln\left(\frac{K_T + K_A V_f^2}{K_T + K_A V_i^2}\right) \tag{3.40}$$

$$K_T = \left(\frac{T}{W}\right) - \mu \tag{3.41}$$

$$K_A = \frac{\rho}{2(W/S_w)}(\mu C_L - C_{D_0} - k_{ind}\, C_L^2) \tag{3.42}$$

Equation 3.40 integrates ground roll from any initial velocity to any final velocity. Since the thrust varies during the ground roll, an averaged thrust value must be used. Since it is

integrated with respect to velocity squared, the averaged thrust to use is the thrust at about 70% of V_{to}.

The ground rolling resistance (μ) is assumed to be the one for a wet asphalt with a value of 0.05. The calculations are done for a take-off height of $500\,m$.

The time to rotate to lift-off attitude depends mostly upon the pilot. A typical assumption for large aircraft is that rotation takes $3\,s$. The acceleration is assumed to be negligible over that short time interval, so:

$$S_{rot} = 3s \cdot V_{to} \tag{3.43}$$

Transition

During the transition, the aircraft accelerates from take-off speed ($1.1\,V_{to}$) to climb speed ($1.2V_{stall}$). The average velocity during transition is therefore about $1.15V_{stall}$. The average lift coefficient during transition can be assumed to be about 90% of the maximum lift coefficient. The average vertical acceleration in terms of load factor (n) can be found in the following equations:

$$n = \frac{L}{W} = \frac{1/2\,\rho S_w (0.9 C_{L_{max}})(1.15 V_{stall})^2}{1/2\,\rho S C_{L_{max}} V_{stall}^2} = 1.2 \tag{3.44}$$

$$n = 1 + \frac{V_{trans}^2}{R_{arc}\,g} = 1.2 \rightarrow R_{arc} = \frac{V_{trans}^2}{0.2g} \tag{3.45}$$

The vertical load factor must be equal to 1 plus the centripetal acceleration required to cause the aircraft to follow the circular transition-arc. The climb angle γ_{climb} at the end of the transition, the horizontal distance traveled during this phase and the height gained is determined from:

$$sin(\gamma_{climb}) = \frac{T - D}{W} \tag{3.46}$$

$$S_{trans} = R_{arc}\,sin(\gamma_{climb}) = R_{arc}\left(\frac{T-D}{W}\right) = R_{arc}\left(\frac{T}{W} - \frac{1}{L/D}\right) \tag{3.47}$$

$$h_{trans} = R_{arc}\,(1 - cos(\gamma_{climb})) \tag{3.48}$$

If the obstacle height is cleared before the end of the transition segment, then Equation 3.49 is used the determine the transition distance.

$$S_{trans} = \sqrt{R_{arc}^2 - (R_{arc} - h_{trans})^2} \tag{3.49}$$

Climb

Finally, the horizontal distance traveled during the climb to clear the obstacle height is found in Equation 3.50. The required obstacle clearance is $35\ ft$ for commercial aviation.

$$S_{climb} = \frac{h_{obstacle} - h_{trans}}{tan(\gamma_{climb})} \tag{3.50}$$

If the obstacle height was cleared during transition, then $S_{climb} = 0$. The following results are obtained:

- $V_{stall} = \sqrt{\frac{W_{to}}{1/2\,\rho\,S_w\,C_{L_{mx}}}} = 67\ m/s$
- $V_{to} = 1.1\,V_{stall} = 73.8\ m/s$
- $V_{trans} = 1.15\,V_{stall} = 77.1\ m/s$
- $S_{Groll} = 1998.7\ m$
- $S_{rot} = 221.27\ m$
- $S_{trans} = 264.33\ m$
- $S_{climb} = 0\ m$
- $\mathbf{S_{to,total} = 2484.3\ m}$

6.2 Landing distance

Landing analysis is similar to the take-off one. The landing distance is divided in three segments: approach, flare and ground roll.

Approach

The approach begins with obstacle clearance over a $50\ ft$ object with an approach speed of $V_{appr} = 1.3\, V_{stall}$ (for commercial). The steepest approach angle is calculated from Equation 3.46.

For transport aircraft, the approach angle should be no steeper than $3°$, which may require more than idle thrust. Approach distance is determined from Equation 3.50 using the flare height h_f.

Flare

Touchdown speed V_{td} is $1.15\, V_{stall}$ (for commercial). The aircraft accelerates from V_{appr} to V_{td}. during flare. The average velocity during the flare is $1.23\, V_{stall}$ The radius of the flare is a circular arc found by Equation 3.45 using V_f and $n = 1.2$. The horizontal distance can be found from Equation 3.47 and the height in Equation 3.48.

Ground Roll

After touchdown, the aircraft rolls free for several seconds before the pilot applies the brakes. The distance is V_{td} times the assumed delay ($2\ s$). The braking distance is determined by the same equation used for take-off ground roll (Equation 3.40), where the initial velocity is V_{td} and the final one is zero. The thrust term is assumed to be zero too. The ground rolling resistance using brakes is assumed to be in wet conditions, so $\mu = 0.3$.

The following results are obtained:

- $V_{appr} = 1.3\, V_{stall} = 80.5\, m/s$
- $V_{td} = 1.15\, V_{stall} = 71.2\, m/s$
- $S_{approach} = 216.1\, m$
- $S_{flare} = 153.6\, m$
- $S_{Froll} = 142.4\, m$
- $S_{Groll} = 1079.3\, m$
- $\mathbf{S_{land,total} = 1591.4\ m}$

7 Restrictions

The performance of the new aircraft is analyzed using the wing loading and the thrust-to-weight ratio for different phases of the flight. Again, **weight units in $\mathbf{Newton}$**.

7.1 Cruise

To maintain a level flight, these forces must be equal:

$$\begin{aligned} L_{cr} &= W_{cr} \\ T_{cr} &= D_{cr} \end{aligned} \tag{3.51}$$

Dividing them, it is obtained:

$$\frac{T_{cr}}{W_{cr}} = \frac{D_{cr}}{L_{cr}} \rightarrow \frac{T_{cr}}{W_{cr}} = \frac{C_{D_0} + k_{ind} \cdot C_{L_{cr}}^2}{C_{L_{cr}}} \tag{3.52}$$

Knowing that $C_{L_{cr}} = \dfrac{W_{cr}/S_w}{q_{cr}}$,

$$\frac{T_{cr}}{W_{cr}} = \frac{C_{D_0} + k_{ind} \left(\frac{W_{cr}/S_w}{q_{cr}}\right)^2}{\frac{W_{cr}/S_w}{q_{cr}}} \tag{3.53}$$

7.2 Take-off

Take-off will be analyzed according to the following expression:

$$\frac{T_{to}}{W_{to}} = k_{to} \cdot \frac{W_{to}/S_w}{\sigma \cdot C_{L_{max,to}} \cdot S_{to}} \tag{3.54}$$

Where k_{to} is a parameter that is obtained through correlations. In this case, the take-off distance was calculated in Section and was adjusted based on that. The conditions analyzed are:

- $C_{L_{max,to}} = 0.9099$

- $k_{to} = 0.202$
- $S_{to} = 2500\,m$
- $z = 500\,m$

7.3 Climb

The minimum thrust-to-weight ratio for the climb phase depends on the climb gradient:

$$\frac{T_{cl}}{W_{cl}} = G + 2\sqrt{C_{D_0} \cdot k_{ind}} \tag{3.55}$$

Where $G = sin(\gamma_{cl})$. As it is a commercial aircraft, $\gamma_{cl} = 0.03$ according to *FAR Part 25* [20]. The Thrust-to-weight ratio must be greater than the minimum with one engine inoperative. The minimum is $\left(\frac{T_{cl}}{W_{cl}}\right)_{min} = 0.067604$, and the real value with only one engine is 0.088587, so the performance is above the restriction.

7.4 Landing

The landing is analyzed in a similar way as the take-off:

$$\frac{W_{to}}{S_w} = \frac{W_{to}}{W_{land}} \cdot k_{land} \cdot \sigma \cdot C_{L_{max_{,land}}} \cdot S_{land} \tag{3.56}$$

Where k_{land} is a parameter that collects all constants (brake efficiencies, type of runway, meteorological conditions, etc. To obtain it, the landing distance is calculated S_{land} and k_{land} is adjusted based on it.

The conditions analyzed for landing are:

- $C_{L_{max,land}} = 0.9099$
- $S_{land} = 1650\,m$
- $k_{land} = 1.49$
- $z = 500\,m$

7.5 Results

The results of this analysis are present in Figure 3.8, where the location of the Design Point can be seen. This point presents a minimized Thrust-to-weight ratio and a high wing loading, which is preferable for its better behavior under gusts and because it tends to minimize the weight of the structure of the aircraft. This point is also located within the acceptable range of takeoff, ascent and landing restrictions.

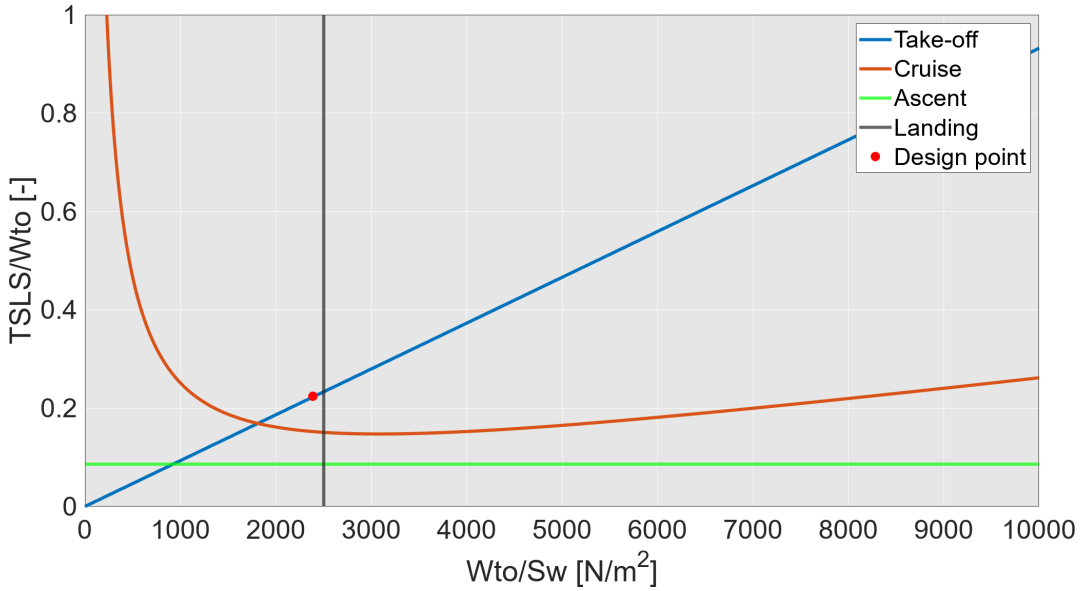

Figure 3.8: Performance (restrictions).

8 Internal dimensioning

The interior of the plane will be designed to accommodate 300 passengers plus the 8 crew members. In Figure 3.9 it can be see how the floors are sized. Above the upper deck the fuel tanks will be placed, while the passengers will go below. Under the lower deck there is a small space that could be used for the storage of suitcases. The lower deck will be at a certain height to offer the maximum surface area for passenger accommodation, while allowing an optimal volume for the hydrogen tanks. The height of the passenger cabin is $2.35\,m$. The width of the decks is $0.3\,m$.

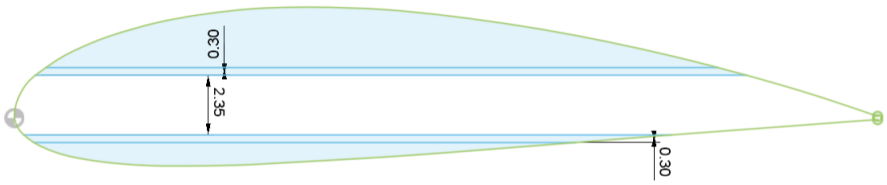

Figure 3.9: Distribution of the floors.

8.1 Passengers cabin

The aircraft is capable of carrying 300 passengers in normal class. The dimensions of the seats are given by Figure 3.10 and Table 3.6. The width of the aisle is $0.6\,m$ and the distance between rows of seats is $0.275\,m$.

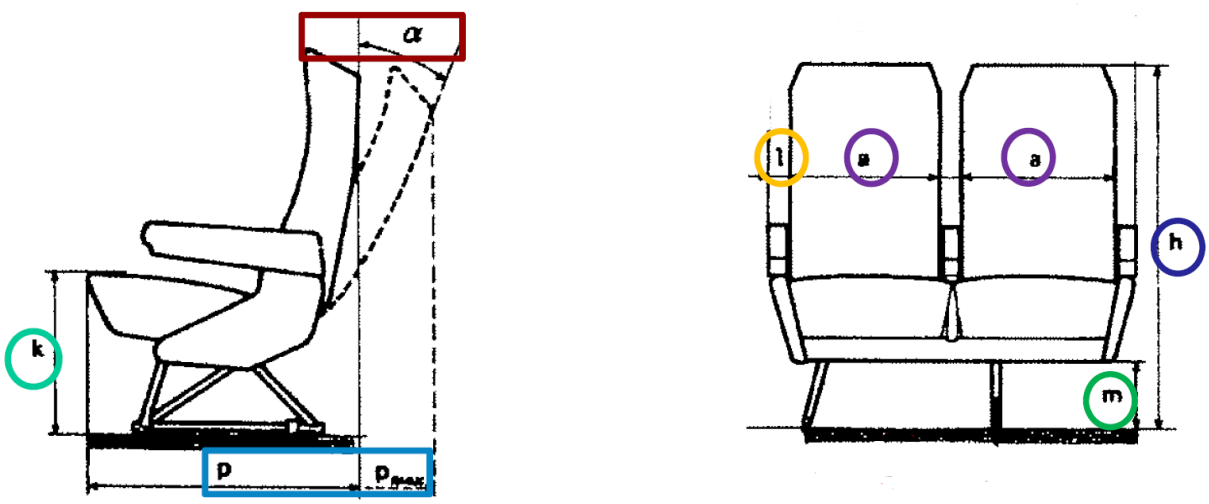

Figure 3.10: Design parameters of the seat.

Parameter	Value
a	0.5 m
l	0.055 m
h	1.07 m
k	0.45 m
m	0.22 m
$p/pmax$	70/95 cm
α/α_{max}	15/38 deg

Table 3.6: Design parameters of the seat.

The aircraft also has a toilet located in the rear area of the cabin. This toilet has four toilets half a meter in diameter, and four sinks. The distribution of half toilet is shown in Figure 3.11. The other half will be symmetric with respect to the middle plane of the aircraft.

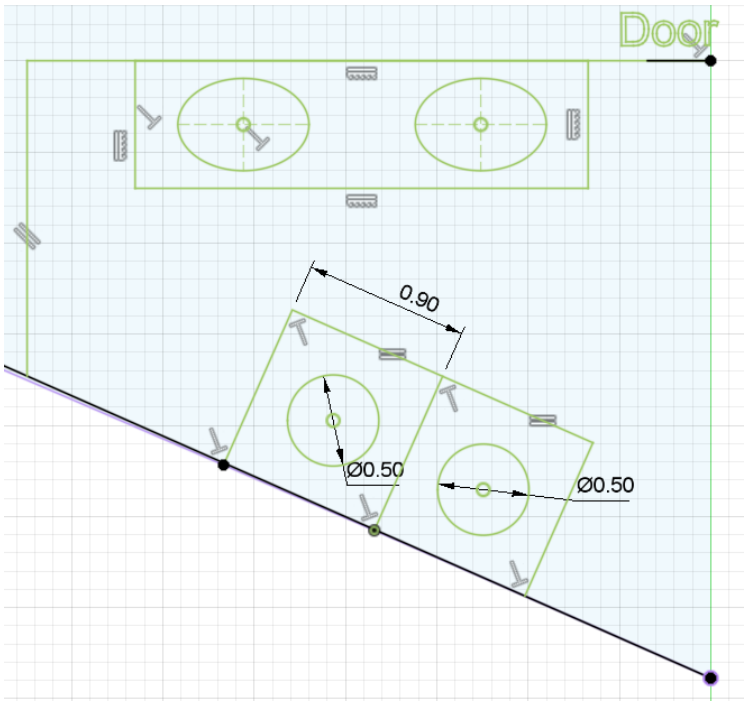

Figure 3.11: Distribution of half toilet.

Figure 3.12 shows the internal distribution of the cabin. It can be seen the dimensions of the seats, the width of the corridors, number of columns and rows, and the toilet. The distribution consists of four columns of three seats per row, and six columns of two seats per row. In addition, there are 6 seats at the rear part for the flight assistants.

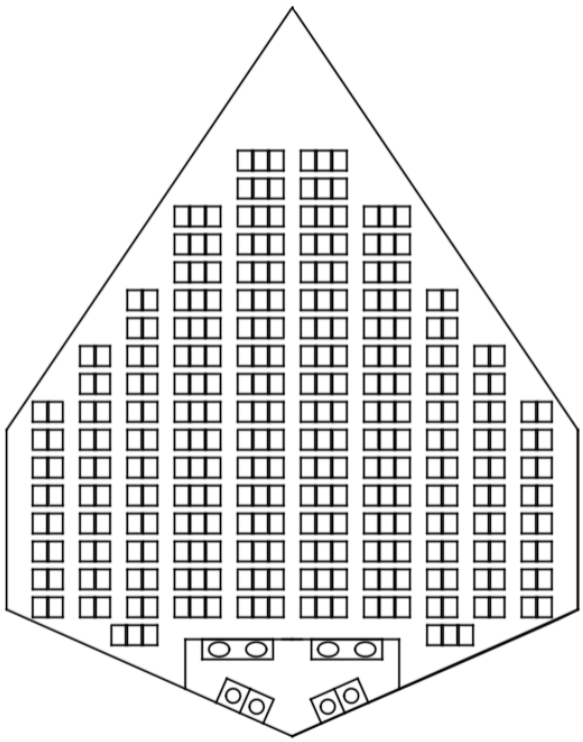

Figure 3.12: Internal distribution of the cabin

8.2 Fuel tanks

The fuel tanks will be placed in three different locations: above the passenger cabin, at the rear and in the blending zone that connects the fuselage with the main wing. The sum of the three volumes must be equal or the greater than the volume of fuel required for the mission.

- Volume at the upper part of the cabin: $V_1 = 307.73\, m^3$
- Volume at the rear part of the cabin: $V_2 = 265.69\, m^3$
- Volume at the blending zone: $V_3 = 122.86\, m^3$
- Total volume available: $V_{tot} = V_1 + V_2 + V_3 = 696.28\, m^3$
- Volume required: $V_{req} = 1.3 \cdot W_{fuel}/\rho_{LH_2} = 563.45\, m^3$

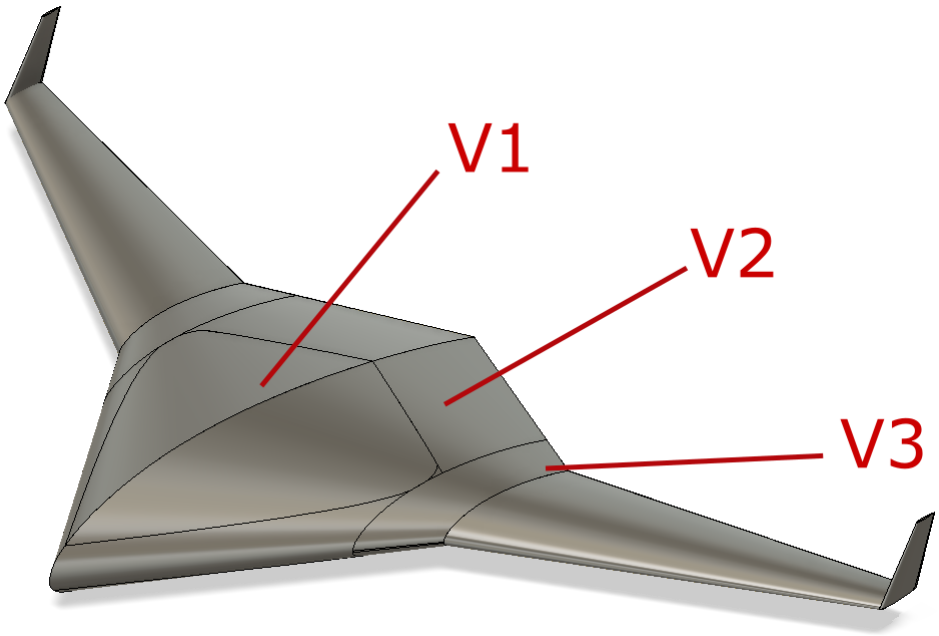

Figure 3.13: Location of the different fuel tanks.

A factor of 1.3 is applied to consider the space occupied by the walls and losses due to the implementation of the tanks. The volume available is $132.83 m^3$ greater than the one required. This excess in volume could be used in the storage of luggage. In addition, the walls of the passengers cabin should be reinforced with fireproof materials to prevent danger in accidents.

9 Estimation of performance

In this section, the performance during cruise will be analyzed. For this purpose, a 500 step simulation will be done, following the same mission as in the reverse engineering. The aircraft will fly at $z_{cr} = 11.5\,km$ and $M = 0.75$. The results are calculated the same way as in the reverse engineering (subsection 3.6), obtaining:

- Endurance in hours (Breguet eq.):

$$E = \sum_{i=1}^{500} \frac{AE_i}{C_i} ln\left(\frac{W_i}{W_{i+1}}\right) = \mathbf{16.33\ h} \tag{3.57}$$

- Range in kilometers (Breguet eq.)

$$R = \sum_{i}^{500} E_i \cdot V_i \cdot \frac{3600}{1000} = \mathbf{13015.65\ km} \tag{3.58}$$

The evolution of several parameters during cruise is also evaluated:

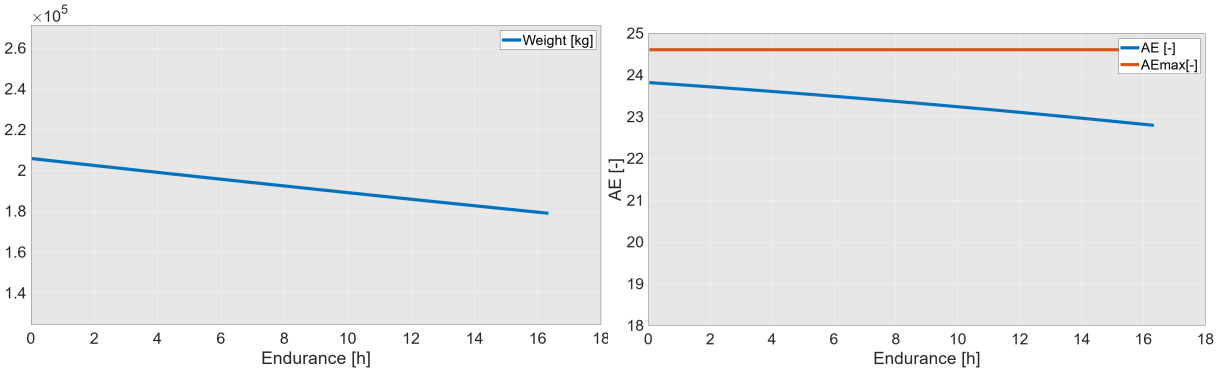

(a) Weight vs Endurance evolution. **(b)** Aerodynamic efficiency evolution in cruise.

Figure 3.14: New design parameter evolutions (I).

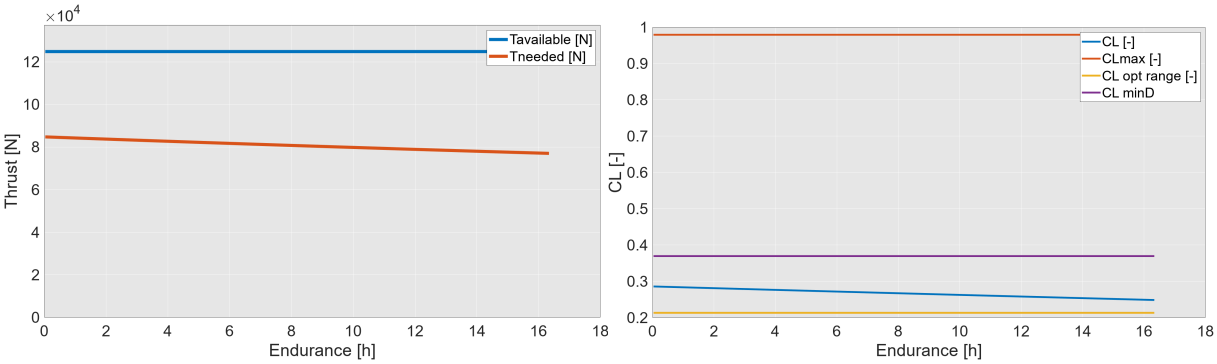

(a) Thrust needed in cruise. **(b)** Evolution of the lift coefficient.

Figure 3.15: New design parameter evolutions (II).

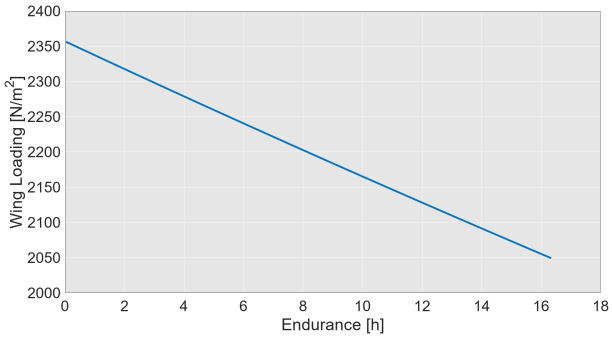

(a) Wing loading evolution

Figure 3.16: New design parameter evolutions (III)

In all of the figures above, a decreasing tendency in time can be seen because of the fuel weight loss, as in the A350-1000 case.

In Figure 3.14, the maximum aerodynamic efficiency is never reached. The reason is that the C_L required for flying is always lower than the one for minimum Drag. However, the aerodynamic efficiency is in a range of values higher than for the A350. It starts with an $AE = 23.81$ and ends with $AE = 22.79$. The maximum efficiency would be $AE_{max} = 24.6$.

Figure 3.15a shows the required thrust (also known as Drag) required for levelled flight, and the force produced by the engine. It decreases with time, but less than in the A350 case as the decrease in weight is lower. The available thrust is much higher than the needed, as the main restriction in the engine selection was the take-off distance. In order to get these two lines closer, the airport runways may be increased in length, so the engine is selected to match in cruise with the drag.

In Figure 3.15b can be seen the lift coefficient evolution. The C_L required in cruise is always lower than the maximum C_L. It starts with a value of $C_L = 0.286$ and ends with $C_L = 0.249$.

CHAPTER 4

Conclusion

The aim of this thesis was to study the influence of the introduction of the hydrogen in the aviation. Due to its negative effect in the performance of the aircraft, the design of a Blended Wing Body aircraft that could counteract some of these effects was considered.

This new configuration consists of the fuselage wing, the main wing and the vertical tails. The fuselage wing design is driven by capacity considerations, while the main wing design will be subject to aerodynamic ones. The vertical tails will be placed at the tip of the main wing and will act as winglets. The pitch control will be provided by some elevons and control surfaces.

The main advantages of the new configuration are increased aerodynamic efficiency and reduced wetted area. The hydrogen tanks can be stored without an aerodynamic penalty. The aerodynamic efficiency is increased by 27%, similar to what Okonkwo et al. studied ($15\% - 20\%$) [11].

The propulsion system was changed. This new configuration requires less thrust in cruise due to better aerodynamics and lower weight. However, for the same thrust, the takeoff distance will be greater, so a more powerful engine is needed. Building longer airport runways should be taken into consideration if all aviation eventually shifts to the Blended Wing Body model. This will enable the engine to run at its most efficient speed by balancing the required and available thrust during cruise.

On the other hand, the performance simulations involved breaking the entire cruise into 500 steps, taking into account weight loss from fuel consumption. In order to simulate a real-world situation and maintain the same conditions for both reverse engineering and new design, a number of assumptions about the overall mission (weight fractions, payload weight, gravimetric index, thrust, consumption models...) were made. The obtained total endurance was $16.33\,h$. This time is for maximum fuel and maximum payload. It could be increased by decreasing payload while maintaining maximum fuel.

With this master thesis, the ability to create a hydrogen aircraft with characteristics similar to those of a Tube and Wing aircraft has been demonstrated. In this case, the A350-1000 was chosen as the reference aircraft, a highly efficient and technologically advanced airplane. The difference in range between this aircraft and the designed one is only $1130\ km$, which is 7.99% of the reference one.

The final design can be seen in Figure 4.1.

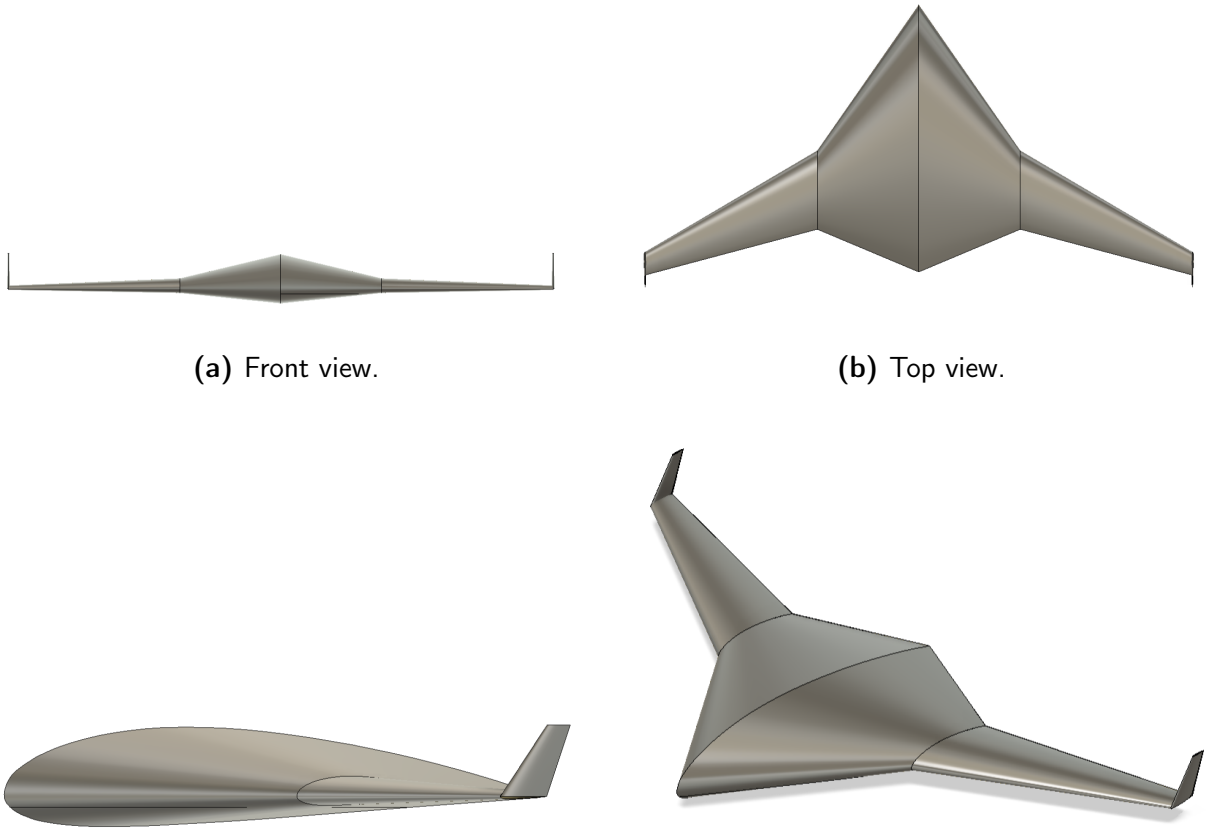

(a) Front view.

(b) Top view.

(c) Side view.

(d) 3D view.

Figure 4.1: Views of the final design.

Bibliography

[1] Clean Sky 2. "Hydrogen-powered aviation". In: (2020). DOI: 10.2843/766989.

[2] Jayant Mukhopadhaya and Dan Rutherford. *PERFORMANCE ANALYSIS OF EVOLUTIONARY HYDROGEN-POWERED AIRCRAFT*. 2022.

[3] Iberdrola. *DIFFERENCE BETWEEN GREEN AND BLUE HYDROGEN*. URL: https://www.iberdrola.com/about-us/what-we-do/green-hydrogen/difference-hydrogen-green-blue#:~:text=The%20main%20difference%20between%20green,model%20based%20on%20fossil%20fuels..

[4] D. Verstraete et al. "Hydrogen fuel tanks for subsonic transport aircraft". In: *International Journal of Hydrogen Energy* 35 (20 Oct. 2010), pp. 11085–11098. ISSN: 03603199. DOI: 10.1016/j.ijhydene.2010.06.060.

[5] ModernAirliners. *Airbus A320*. URL: https://modernairliners.com/airbus-a320-introduction/airbus-a320-specs/.

[6] Wikipedia. *Airbus A350*. URL: https://en.wikipedia.org/wiki/Airbus_A350#Specifications.

[7] Élodie Roux. *Turbofan and Turbojet Engines: Database Handbook*. Blagnac, France, 2007.

[8] D. Verstraete. *On the energy efficiency of hydrogen-fuelled transport aircraft*. 2015.

[9] Egbert Torenbeek. *Blended Wing Body Aircraft: A Historical Perspective*. May 2016. DOI: 10.1002/9780470686652.eae1003.

[10] Zhenli CHEN et al. "Assessment on critical technologies for conceptual design of blended-wing-body civil aircraft". In: *Chinese Journal of Aeronautics* 32 (8 Aug. 2019), pp. 1797–1827. ISSN: 10009361. DOI: 10.1016/j.cja.2019.06.006.

[11] Paul Okonkwo and Howard Smith. *Review of evolving trends in blended wing body aircraft design*. Apr. 2016. DOI: 10.1016/j.paerosci.2015.12.002.

[12] Aerospace-Technology. *Airbus A350-1000 Aircraft*. URL: https://www.aerospace-technology.com/projects/airbus-a350-1000-aircraft/.

[13] AviacionDigital. *Diez nuevos Airbus A350-1000 y cinco A350-900 para Lufthansa*. URL: https://aviaciondigital.com/diez-nuevos-airbus-a350-1000-y-cinco-a350-900-para-lufthansa/.

[14] Airbus A350. *Wings*. URL: http://www.airbus-a350.com/the-aircraft/wings.php.

[15] Airbus. *A350. Less Weight. Less Fuel. More Sustainable.* URL: https://aircraft.airbus.com/en/aircraft/a350-clean-sheet-clean-start/a350-less-weight-less-fuel-more-sustainable.

[16] Military Factory. *Boeing X-48*. URL: https://www.militaryfactory.com/aircraft/detail.php?aircraft_id=1338.

[17] NASA. *Past Projects: X-48B Blended Wing Body*. URL: https://www.nasa.gov/centers/dryden/research/X-48B/index.html.

[18] AIRBUS. *Imagine travelling in this blended wing body aircraft*. URL: https://www.airbus.com/en/newsroom/stories/2020-11-imagine-travelling-in-this-blended-wing-body-aircraft.

[19] XATAKA. *Airbus desvela el Maveric, un sorprendente avión de ala integrada con el que quiere revolucionar la aviación comercial*. URL: https://www.xataka.com/vehiculos/airbus-desvela-maveric-sorprendente-avion-ala-integrada-que-quiere-revolucionar-aviacion-comercial.

[20] Thomas C. Corke. *Design of aircraft*. Prentice Hall, 2003.

[21] Daniel P. Raymer. *Aircraft design: A conceptual approach*. American Institue of Aeronautics and Astronautics, 1992.

[22] Airfoil Tools. *Airfoil database search*. URL: http://airfoiltools.com/search/index.

[23] Nita. *Estimating the Oswald Factor from Basic Aircraft Geometrical Parameters*. 2012.

[24] Marcos Carreres. "Propulsion models". In: *Universitat Politècnica de València* (2020).

[25] R. H. Liebeck. *Design of the BlendedWing Body Subsonic Transport*. 2004.

[26] Toshihiro Ikeda and Cees Bil. *AERODYNAMIC PERFORMANCE OF A BLENDED-WING-BODY CONFIGURATION AIRCRAFT*.

[27] Kevin R Bradley. *A Sizing Methodology for the Conceptual Design of Blended-Wing-Body Transports*. URL: http://www.sti.nasa.gov.

[28] Aircraft Aerodynamics and Design Group 2004. *Component Weights*. 2004.

[29] UPV Marcos Carreres. *0.2 Some basic notions about Aerodynamics*.

[30] Dave Dargie. *How long is an airport's runway?* URL: https://www.stantec.com/en/ideas/topic/mobility/how-long-is-an-airport-s-runway#:~:text=Between%20these%20two%20runway%20extremes,13%2C000%20feet%20(3%2C962%20meters)..